ACS OMEGA

Open Access

http://pubs.acs.org/journal/acsodf

Article

Engineering of the Central Core on DBD-Based Materials with Improved Power-Conversion Efficiency by Using the DFT Approach

Published as part of ACS Omega virtual special issue "At the Speed of Light: Recent Advances in Optoelectronics".

Aamna Zulfiqar, Muhammad Salim Akhter,* Muhammad Waqas, Ijaz Ahmad Bhatti,* Muhammad Imran, Ahmed M. Shawky, Mohamed Shaban, Hadil Faris Alotaibi,* Ahmed Mahal,* Adel Ashour, Meitao Duan,* Ali S Alshomrany, and Rasheed Ahmad Khera*

Cite This: *ACS Omega* 2024, 9, 29205−29225

Read Online

ACCESS | Metrics & More | Article Recommendations

ABSTRACT: Developing proficient organic solar cells with improved optoelectronic properties is still a matter of concern. In the current study, with an aspiration to boost the optoelectronic properties and proficiency of organic solar cells, seven new small-molecule acceptors (Db1−Db7) are presented by altering the central core of the reference molecule (DBD-4F). The optoelectronic aspects of DBD-4F and Db1−Db7 molecules were explored using the density functional theory (DFT) approach, and solvent-state calculations were assessed utilizing TD-SCF simulations. It was noted that improvement in photovoltaic features was achieved by designing these molecules. The results revealed a bathochromic shift in absorption maxima (λ_{max}) of designed molecules reaching up to 776 nm compared to 736 nm of DBD-4F. Similarly, a narrow band gap, low excitation energy, and reduced binding energy were also observed in newly developed molecules in comparison with the pre-existing DBD-4F molecule. Performance improvement can be indicated by the high light-harvesting efficiency (LHE) of designed molecules (ranging from 0.9992 to 0.9996 eV) compared to the reference having a 0.9991 eV LHE. Db4 and Db5 exhibited surprisingly improved open-circuit voltage (V_{OC}) values up to 1.64 and 1.67 eV and a fill factor of 0.9198 and 0.9210, respectively. Consequently, these newly designed molecules can be considered in the future for practical use in manufacturing OSCs with improved optoelectronic and photovoltaic attributes.

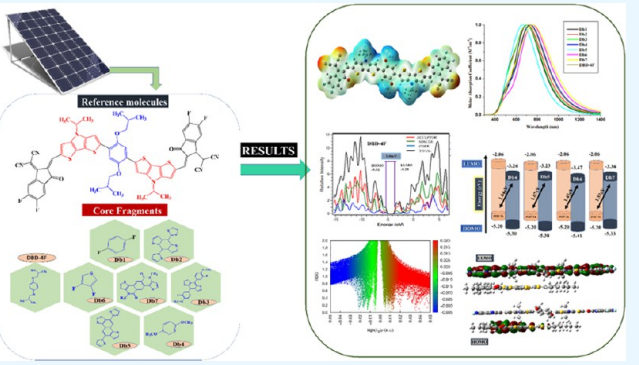

1. INTRODUCTION

Organic solar cells (OSCs) have attracted huge attention and substantial research because of their flexibility, transparency, low production cost, easily tunable energy levels, and potential for high efficiency. OSCs possess several advantages that make them highly versatile in the field of photovoltaics. Their semi-transparency, ability for mass production, and lightweight nature contribute to their broader range of applications.[1−3] Organic photovoltaic cells have achieved a remarkable increase in efficiency, with the engaging donor−acceptor bulk hetero-junction (BHJ) having an increased surface area between the acceptor−donor interface.[4] At present, the major progress in the realm of OSCs is the implementation of nonfullerene-based solar cells. Nonfullerene acceptor-based OSCs show promising potential in replacing fullerene-based OSCs. This is due to their superior photovoltaic characteristics, which include adjustable energy levels, enhanced thermal stability, and a wider absorption range. However, increasing the open-circuit voltage, improving charge mobility, enhancing light-harvesting efficiency, and reducing binding energy are still key concerns for scientists to improve the efficiency of nonfullerene organic solar cells.[5−11]

Nevertheless, there is an immense need to escalate OSCs' efficiency to meet commercial applications' demands. Thus, modifications are done in various fragments of organic solar cells to increase their efficiency. Gao and co-workers in 2021 reported two novel molecules, NCIC and NOCIC, with unfused cores, i.e., pyrazine and pyridazine, attached to two CPDT fragments and 2F-IC as acceptor units. The nitrogen in pyrazine and pyridazine can form noncovalent interactions with sulfur and

Received: November 18, 2023
Revised: January 27, 2024
Accepted: February 20, 2024
Published: March 18, 2024

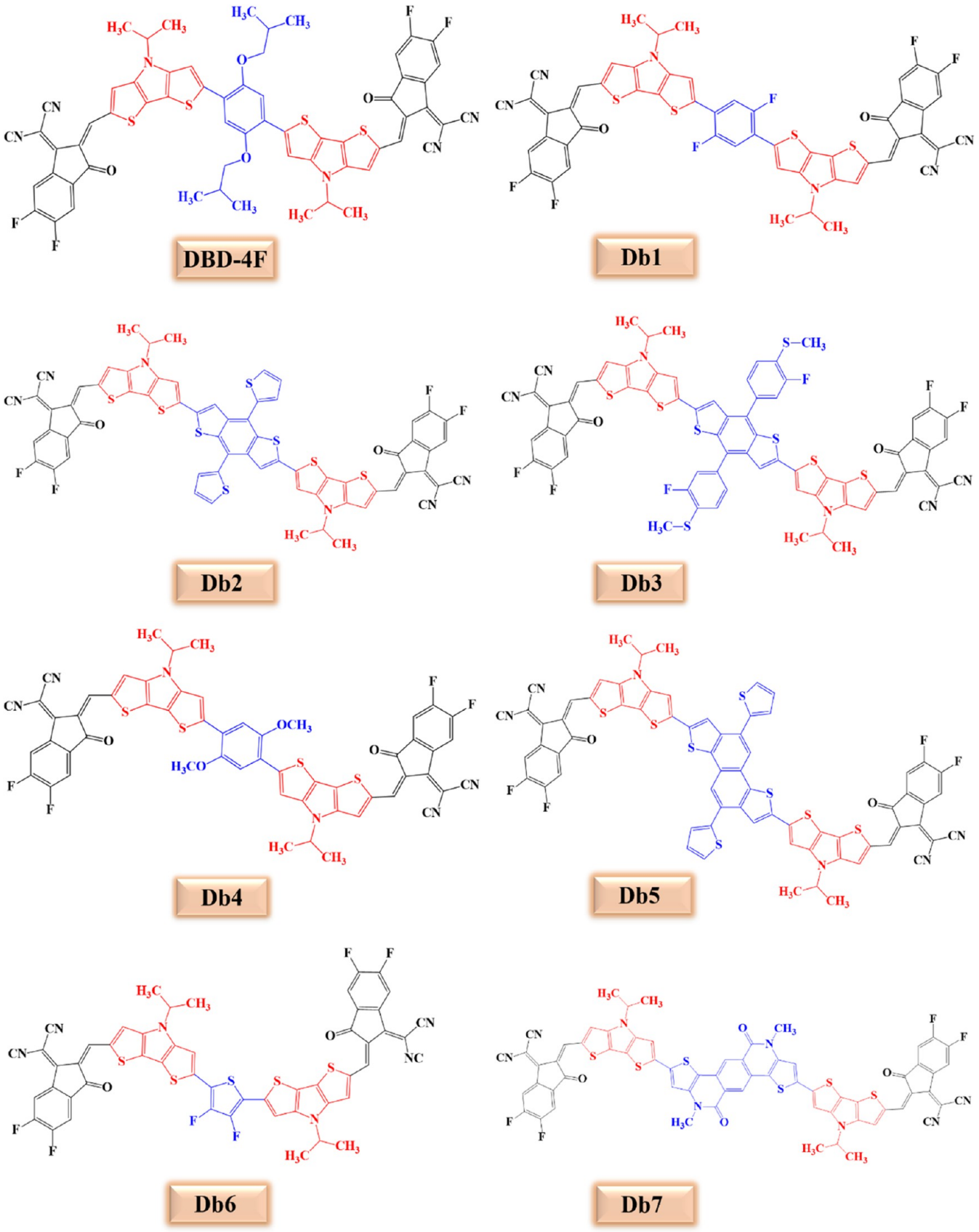

Figure 1. Representation of all molecular structures of DBD-4F and the modified molecules.

hydrogen of the CPDT unit as N···S and N···H. These noncovalent intramolecular interactions expand the conjugated framework, manifest the intense absorption in the near-IR region, and proclaim higher power-conversion efficiency.[12,13]

https://doi.org/10.1021/acsomega.3c09215
ACS Omega 2024, 9, 29205−29225

Recently, remarkable progress has been observed in improving the efficiency of OSCs in different research works. Liu et al. achieved a net power-conversion efficiency (PCE) of 18.26%, forming a blend of PM6:L8-BO:BR-C12.[14] Similarly, Fu and co-workers significantly minimized nonradiative recombination loss in the PM6:BTP-eC9 blend and reported a PCE of 19.31%.[15] Moreover, in an attempt to increase the absorption range of solar materials, Gu and co-workers have recently achieved a PCE of 20.6% in 2T-TSC-based OSCs.[16] By improving the collection and utilization of excitons near electrodes, Ma and co-workers have achieved an efficiency of up to 18.1%.[17]

The fused ring nonfullerene acceptors have electron-withdrawing fragments bond together through an electron-donating core to construct the heavy ladder-like skeleton. However, they are not cost-effective and have great synthetic complexity, which impedes their large-scale synthesis and commercialization. Nonfused ring electron acceptors (NFREAs) linked by single bonds are attractive to OSCs due to their low cost and simplified synthesis process compared to those of their fused ring counterparts. Furthermore, their energy levels and absorption range can be finely tuned.[18,19]

In 2021, Cao and co-workers synthesized three unfused acceptors, including DBT-4F, DBD-4F, and DBTD-4F, by replacing the fragments of highly efficient FREAs (fused ring electron acceptors) to escalate the optoelectronic properties regarding unfused acceptors. These three novel moieties exhibited slender optical band gaps below 1.45 eV. Furthermore, to upgrade the photovoltaic performance, they blended the designed molecules with polymer donor PBDB-T, which proved to be the most competent to expedite efficient charge transfer. Hence, DBT-4F achieved the best performance having a V_{oc} of 0.88 V with an FF of 70.24 and a 12.14% PCE with polymer donor PBDB-T. This PCE was the best-achieved value among unfused acceptors. An asymmetric framework of type A-D_1-D-D_2-A in DBT-4F manifested the planarity of a high degree owing to noncovalent intramolecular interactions such as O···S and O···H.[20,21] On the other flip, DBD-4F bears a symmetric framework, i.e., A-D_1-D-D_1-A, which requires a distortion of the structure and replaces the segments with more efficient fragments to ameliorate the parameters of V_{oc}, FF, E_g, hole and electron charge transfer, dipole moment, and light-harvesting efficiency (LHE).[13]

In the current study, seven new molecules are designed by the core modification of the DBD-4F molecule. The central core of DBD-4F was replaced with 1,4-difluoro-benzene in the Db1 molecule, 4,8-dithiophen-2-yl-3*a*,4,4*a*,7*a*,8,8*a*-hexahydro-1,5-dithia-*s*-indacene in the Db2 molecule, 4,7-bis(3-fluoro-4-methylsulfanyl-phenyl)-6-methyl-benzo[*b*]thiophene-5-thiol in the Db3 molecule, 1,4-dimethoxy-2-methyl-benzene in the Db4 molecule, 5,10-dithiophen-2-yl-3,8,dithia-dicyclopenta[*a*,*f*]-naphthalene in the Db5 molecule, 3,4-difluoro-thiophene in the Db6 molecule, and 4,10-dimethyl-4,10-dihydro-1,7-dithia-4,10-diaza-dicyclopenta[*a*,*h*]anthracene-5,11-dione in the Db7 molecule. All of the previously mentioned molecules (Db1−Db7) have the same acceptor (5,6-difluoro-3-oxo-indan-1-ylidene)-isocyano-acetonitrile and spacer (4-isopropyl-4*H*-dithieno[3,2-b;2′3′-*d*] pyrrole). The designed molecules can be manufactured by synthesizing the central core in the first step. Then, already available spacers and acceptors can be attached with central cores in the presence of suitable catalysts, as explained in the literature.[22] Figure 1 depicts the structural representation of all of these molecules. This study aims to increase the optical and electronic characteristics of DBD-4F (reference molecule), which can be done by using these central cores. These central cores can boost the different photovoltaic parameters of nonfullerene OSCs.[23,24]

2. COMPUTATIONAL DETAILS

The Gaussian 09W[25] program was employed to complete quantum mechanical investigations with Gauss View 6.0[26] to visualize the results. Geometrical optimization of reference molecule DBD-4F was done with the aid of four particular exchange−correlation functionals; B3LYP,[27] CAM-B3LYP,[28] MPW1PW91,[29] WB97XD[30] at the 6-31G(d,p) basis set of density functional theory (DFT) theory.[31] TD-SCF computations were carried out to generate an absorption spectrum for reference molecules in the solvent (chloroform) medium and the gaseous phase. The solvent effect on molecules' electronic and optical properties is observed using the IEFPCM.[32] Furthermore, absorption spectra comparison of these four functionals B3LYP (736 nm), CAM-B3LYP (545 nm), MPW1PW91 (688 nm), and WB97XD (521 nm) with experimental one of DBD-4F revealed that the λ_{max} of 736 nm for B3LYP proclaimed the closest value to reported λ_{max} (731 nm). Thus, the accepted B3LYP is the best fit for further theoretical work. Thus, all observations of newly purposed molecules are calculated at B3LYP on the basis set 6-31G(d,p). TD-SCF was employed to examine the UV−visible absorption spectra of all designed compounds for which the graph is plotted through the Origin 6.0 program,[33] as shown in Figure 2.

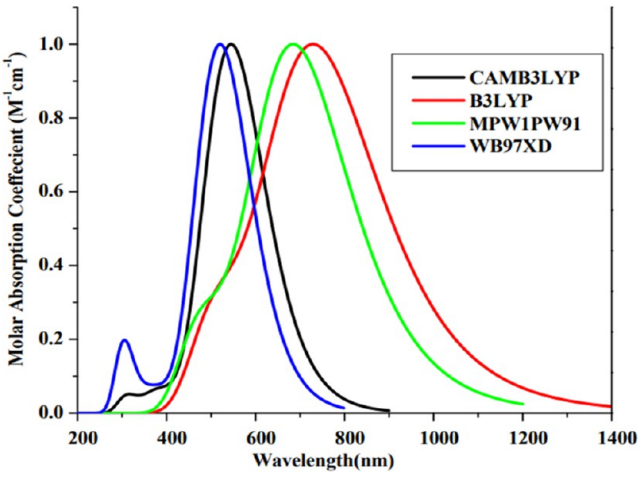

Figure 2. Absorption spectra of DBD-4F with four discrete functionals in the chloroform solvent.

Moreover, using Multiwfn (multifunctional wave function) 3.8 software,[34] TDM graphs are plotted that indicate the nature of excitations and transitions of electrons. Using PyMOlyze 1.1 version software,[35] graphs of DOS have been plotted. Finally, the internal reorganization energies of the hole and electrons of all proposed molecules (Db1−Db7) and DBD-4F are executed by using eqs 1 and 2.[36]

$$\lambda_e = [(E_-{}^0) - (E_0)] + [(E_0{}^-) - (E_-)] \quad (1)$$

$$\lambda_h = [(E_+^0) - (E_0)] + [(E_0{}^+) - (E_+)] \quad (2)$$

where E_+^0 and E_-^0 represent the ground-state energies of the optimized cation and anion calculated at the neutral charge state. E_0 shows the energy calculated at the zero charge state from the

https://doi.org/10.1021/acsomega.3c09215
ACS Omega 2024, 9, 29205−29225

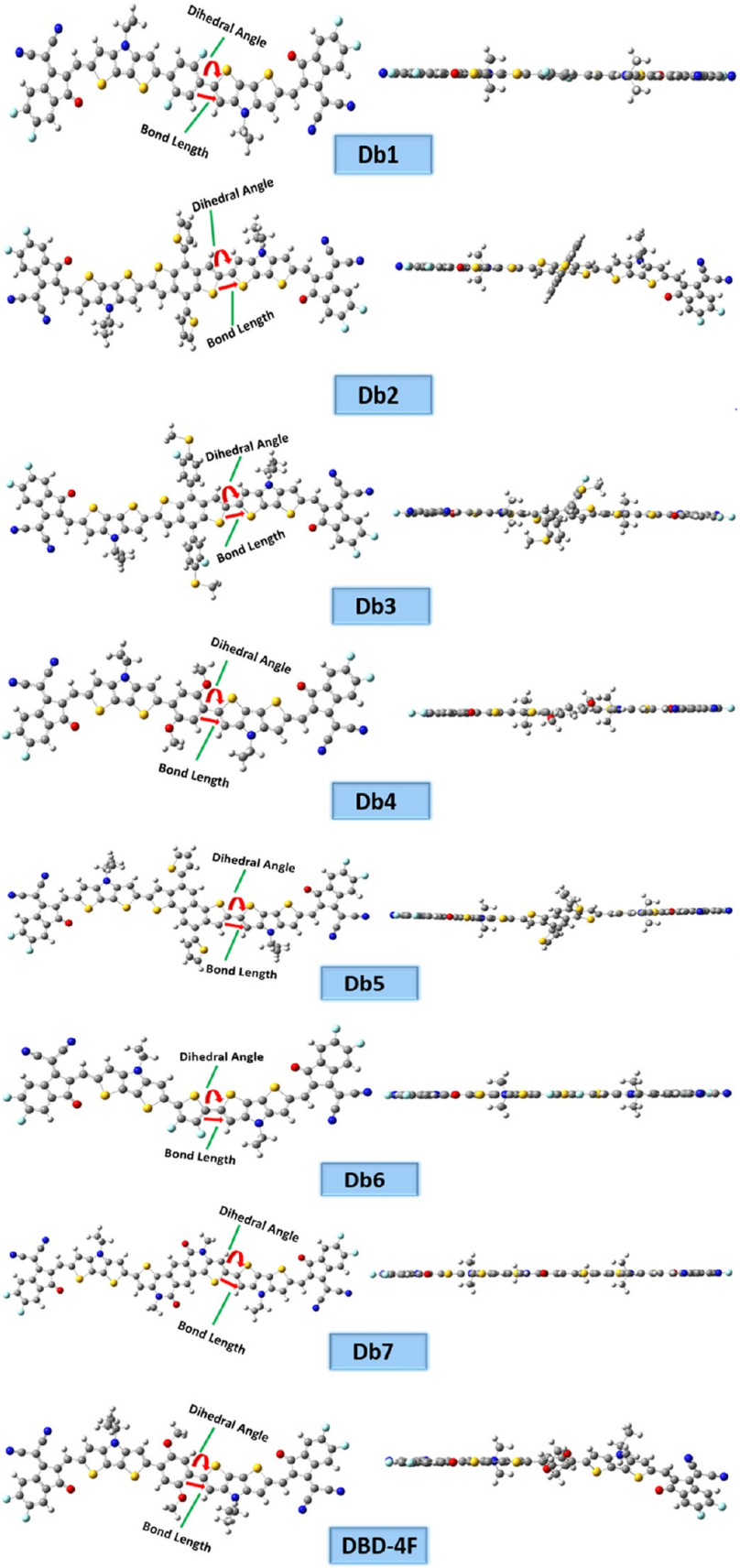

Figure 3. Front and side views of the optimized geometries of reference and all designed moieties.

neutral optimized structures. E_0^- and E_0^+ represent energies of optimized molecules calculated at −1 and +1 charge,

https://doi.org/10.1021/acsomega.3c09215
ACS Omega 2024, 9, 29205−29225

respectively. E_+ denotes the energy of the cation calculated at a +1 charge state and E_- corresponds to the energy of optimized anions calculated at a −1 charge state.[37,38]

3. RESULTS AND DISCUSSION

3.1. Optimized Geometry and Planarity. The ground-state geometry optimization of molecules is crucial to studying the optoelectronic properties in the excited states. Therefore, all of the elaborated chromophores were optimized using the 6-31G(d,p) basis set using the B3LYP functional at the ground state. To evaluate the calculations of the planarity and charge transfer, various important parameters were studied. The bond length and the dihedral angle are important parameters for analyzing conjugation within the molecules.[39] The respective bond lengths and dihedral angles are shown in Figure 3 and Table 1. The bond length within the carbon atoms of central cores and the adjacently attached spacer units of all of the designed and reference molecules fall between 1.43 and 1.45 Å. It lies between the single bond (1.54 Å) and double bond (1.34 Å) lengths between the carbon atoms. This manifests noticeable conjugation among the newly designed molecules. Results demonstrate that the dihedral angles between cores and adjacent spacers lie within the range of 0.43−25.26°.

Table 1. Bond Parameters of Reference and Designed Molecules and Representation of the Span of Deviation from Planarity (SDP) and the Molecular Planarity Parameter (MPP)

molecules	bond length (L_{c-c}) (Å)	bond angle (θ°)	MPP (Å)	SDP (Å)
DBD-4F	1.45	0.434	0.9590	4.9410
Db1	1.44	4.459	0.0520	0.4100
Db2	1.44	9.347	0.9760	4.7120
Db3	1.44	23.49	0.8640	4.9560
Db4	1.45	15.81	0.1830	1.4610
Db5	1.44	25.26	0.7270	4.2950
Db6	1.43	0.009	0.0004	0.0218
Db7	1.43	0.717	0.0965	0.9906

The Db3−Db5 molecules exhibit slightly higher dihedral angles, indicating their deviation from the main plane that might aid in retaining charge density within their fragments after intramolecular charge transfer. However, Db3 and Db5 manifested higher dihedral angles due to the massive donor cores attached, whereas Db4 has bulky electron-donating methoxy groups. In contrast, all other studied molecules have more planar geometry, as their dihedral angles are closer to zero. The Db6 molecule has the lowest value of the dihedral angle (0.009°) and SDP (0.0218 Å), which means that Db6 molecules possess the highest planarity. Higher planarity assists in the smooth transfer of charges, which increases the charge mobility within a molecule.

To determine the effect of donor cores on planarity, the span of deviation from the plane (SDP) and the molecular planarity parameter (MPP) were computed by utilizing Multiwfn 3.8 software, and results were displayed by VMD 1.9 software.[40] These structures are shown in Figure 4. The lower the MPP and SDP values, the higher the molecules' planarity, indicating easy and better charge transfer. All structures show similar planarity because of their comparable MPP values. The MPP and SDP values for reference are 0.959 and 4.941 Å, respectively. Almost all designed molecules have lower values for MPP and SDP, representing improved planarity compared to the reference

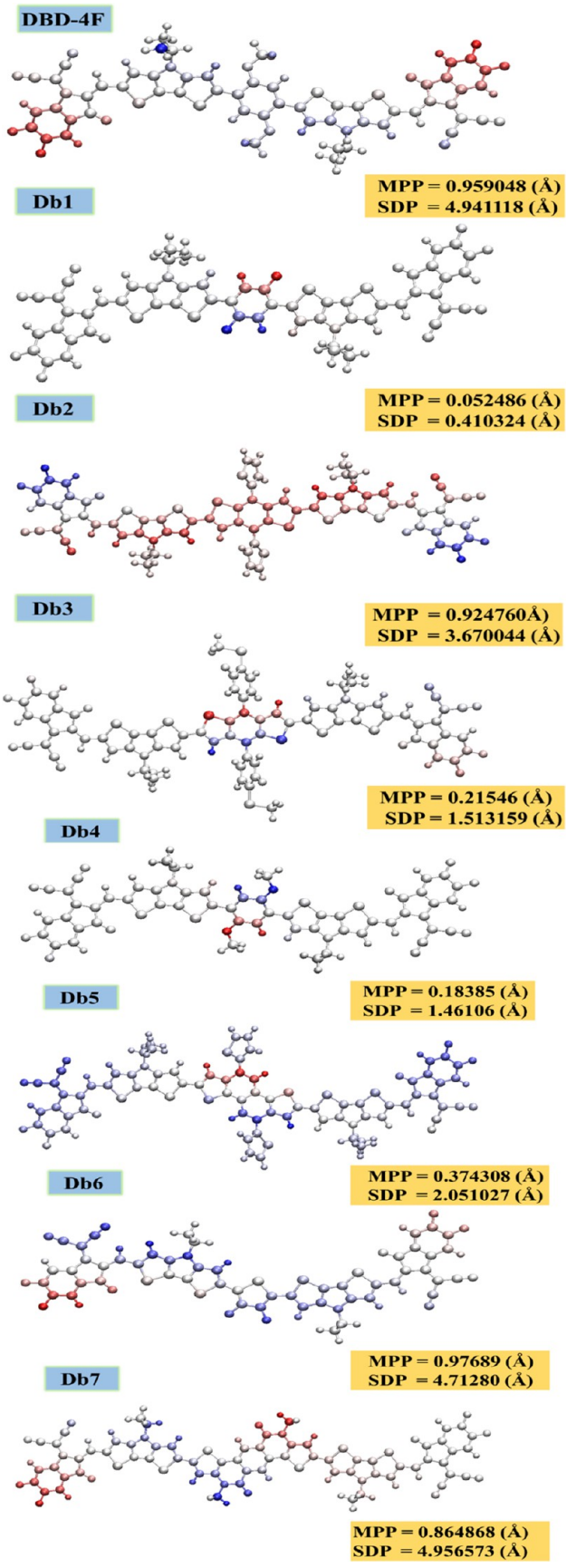

Figure 4. Representation of planarity among all reference and designed molecules.

https://doi.org/10.1021/acsomega.3c09215
ACS Omega 2024, 9, 29205−29225

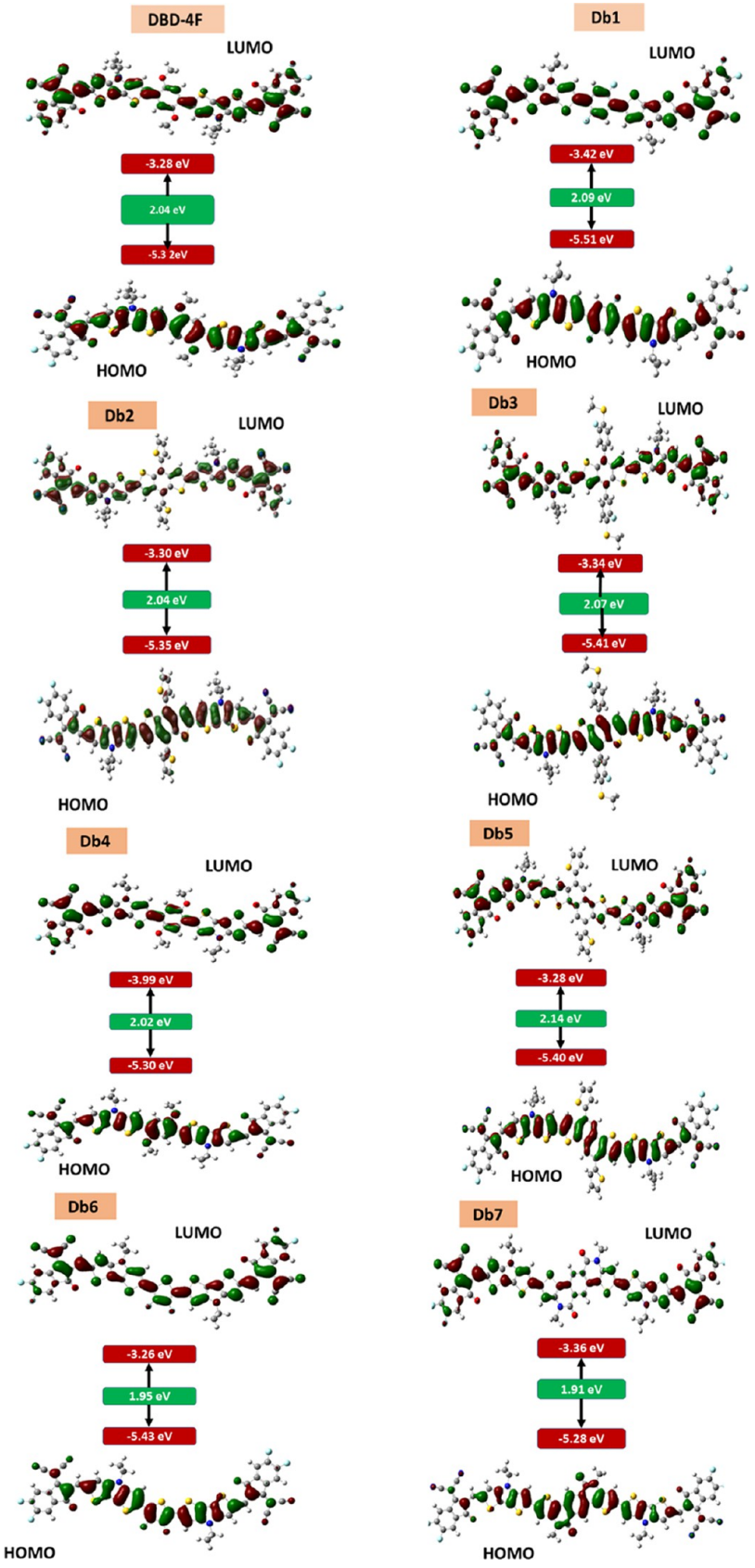

Figure 5. Representation of HOMO and LUMO of reference, designed molecules, and associated band gaps among them.

molecule. Db6 shows the highest planarity, with an MPP value of 0.0004 Å. Db3 shows the highest deviation from the plane, with an SDP value of 4.9560 Å. In a comparison of Db2 with the reference, the SDP and MPP values are quite comparable; Db2 is more planar, leading toward better charge transfer. Thus, these

https://doi.org/10.1021/acsomega.3c09215
ACS Omega 2024, 9, 29205−29225

planar structures can cause effective transfer of charges, which leads to improved efficiency in these newly designed molecules.

3.2. Frontier Molecular Orbital Study. The distribution pattern of frontier molecular orbitals (FMOs) is used to study the optical and electrical properties of all planned compounds. HOMO (highest occupied molecular orbital) and LUMO (lowest unoccupied molecular orbitals) are stated as FMOs.[41−43] Acknowledging FMOs is essential because it provides details on how charges transit from the ground to the excited state. Electrons are located at the HOMO energy level in the ground state. They become excited and migrate toward higher energy orbitals after receiving energy from photons. As an outcome upon excitation, HOMO can move electrons in the direction of LUMO, which takes these excited electrons. Molecules with smaller band gaps are flexible, reactive, and have a fast rate of intramolecular charge transfer.[44] Energy levels of HOMO−LUMO and the band gap of corresponding molecules were investigated at the B3LYP functional to assess the impact of inserting various core subunits on the DBD-4F molecule, as shown in Figure 5. The designed compounds (Db1−Db7) comprise the same terminal subunits and different central core units with their capacity to donate electrons to electron-pulling spacers that extend the length of conjugation and aid in the delocalization of electrons across the surface of molecules.[45]

As shown in Table 2, the calculated energy values of HOMO for reference and all fabricated molecules (Db1−Db7) are

Table 2. Calculated Values of HOMO and LUMO of the Reference and All Designed Molecules with Associated Band Gaps

molecules	E_{HOMO} (eV)	E_{LUMO} (eV)	E_g (eV)
DBD-4F	−5.32	−3.28	2.03
Db1	−5.51	−3.42	2.09
Db2	−5.35	−3.30	2.04
Db3	−5.41	−3.34	2.07
Db4	−5.30	−3.99	2.02
Db5	−5.40	−3.28	2.14
Db6	−5.43	−3.26	1.95
Db7	−5.28	−3.36	1.91

−5.32, −5.51, −5.35, −5.41, −5.30, −5.40, −5.43, and −5.28 eV, respectively. On the other hand, the calculated energy values of LUMO for reference and all newly designed molecules (Db1−Db7) are −3.28, −3.42, −3.30, −3.34, −3.99, −3.28, −3.26, and −3.36 eV, respectively. Collectively, the established band gap was in the order of Db5 > DB1 > Db3 > Db2 > DBD-4F > Db4 > Db6 > Db7. Db7 has the highest lying HOMO energy level at −5.28 eV, which indicates the easier transfer of charges from HOMO to LUMO. Because the low-lying LUMO and high-lying HOMO energy levels cause a reduction in the band gap, it turns out in easier charge transfer from HOMO to LUMO. Compared to the reference molecule, Db4, Db6, and Db7 molecules have a lower energy gap. These results show that D7 has the lowest energy gap due to the existence of fused conjugated rings and additional electronegative atoms in the central core (acridine's), which makes it more suitable for the development of proficient OSCs.

The particularly potent naphthodithiophene (NDT) group accounts for a larger band gap of Db5 than the reference molecule DBD-4F. NDT groups do not have the strong potential to withdraw electrons from their adjacent donors due to the absence of electron-withdrawing groups; therefore, they behave as a donor group. Db6 molecule exhibits the lowest band gap due to the functionality of the core; i.e., robust electron-withdrawing fluorine atoms are attached to the thiophene ring that withdraws electrons from surrounding subunits and thus manifests a high opportunity for electronic transitions. Higher planarity of the Db6 molecule can also assist in easier transfer of charges. Db7 shows a lower band gap than the reference molecule due to the existence of 4,10-dimethyl-4,10-dihydro-1,7-dithia-4,10-diaza-dicyclopental[*a*,*h*]anthracene-5,10-dione that contains highly electronegative nitrogen and oxygen atoms. This large core causes high conjugation and $\pi-\pi$ interactions among the adjacent substituents.

As illustrated in Figure 5, LUMO shows an equal distribution of electron densities on the core component, spacer units, and surrounding acceptor fragments. In contrast, HOMO shows a substantial amount of charge dispersion on the core section, somewhat on the neighboring spacer ring, and to some extent on the terminal acceptor groups. Overall, the electron delocalization sequence is produced due to the distribution of electron density in all of these molecules. The phenomenon of charge transfer from the donor to the acceptor regions makes them a suitable candidate for practical applications in the future.

3.3. Natural Transition Orbitals. Natural transition orbitals (NTOs) are explored to evaluate the extent of successful charge conveyance from the ground state to the excited state. Hence, in order to precisely scrutinize the transfer phenomenon of electrons from HOMO to LUMO, NTOs enact a significant role in determining ETC (electron transfer contribution). Furthermore, it relies on the scattering of HOMO and LUMO over the molecule, which explicitly shows the extent of charges transferring from electrons to holes, as shown in Figure 6.[46,47]

Figure 6 shows that HOMO charge density is only localized on donor fragments, while LUMO charge density is mainly present on acceptor moieties. This separation of HOMO and LUMO charge density indicates the proficient charge transfer from occupied to unoccupied orbitals after charge excitation. The computed values of ETC are listed in Table 6. In all designed molecules, Db6 has the highest percentage of ETC (99.27%) than DBD-4F (99.01%) and all other fabricated molecules. Results show that "3,4-difluorothiophene" in Db6 performs better to transport the charges from the central region to the peripheries. It can be observed that all of the other molecules also possess significant values of %ETC, which makes them useful candidates to uplift the efficiency of photovoltaic cells.

3.4. Ionization Potential and Electron Affinity. The electrochemical characteristics of a molecular structure are thought to be influenced by several important parameters, including the ionization potential (IP) and electron affinity (EA). These two parameters are related to the border orbitals in a significant way. Chromophores with high EA and low IP values accelerate the charge transfer process.[48] A higher value for EA makes injecting electrons into unoccupied LUMO easier, whereas a smaller IP lowers the hole−injection barrier.[49,50] The ionization potential and electron affinity values for planned molecules are calculated by eqs 3 and 4.[51]

$$\mathrm{IP} = [E_0^{+} - E_0] \tag{3}$$

$$\mathrm{EA} = [E_0 - E_0^{-}] \tag{4}$$

For DBD-4F and Db1−Db7 molecules, the computationally calculated IP and EA values are listed in Table 3. All designed

https://doi.org/10.1021/acsomega.3c09215
ACS Omega 2024, 9, 29205−29225

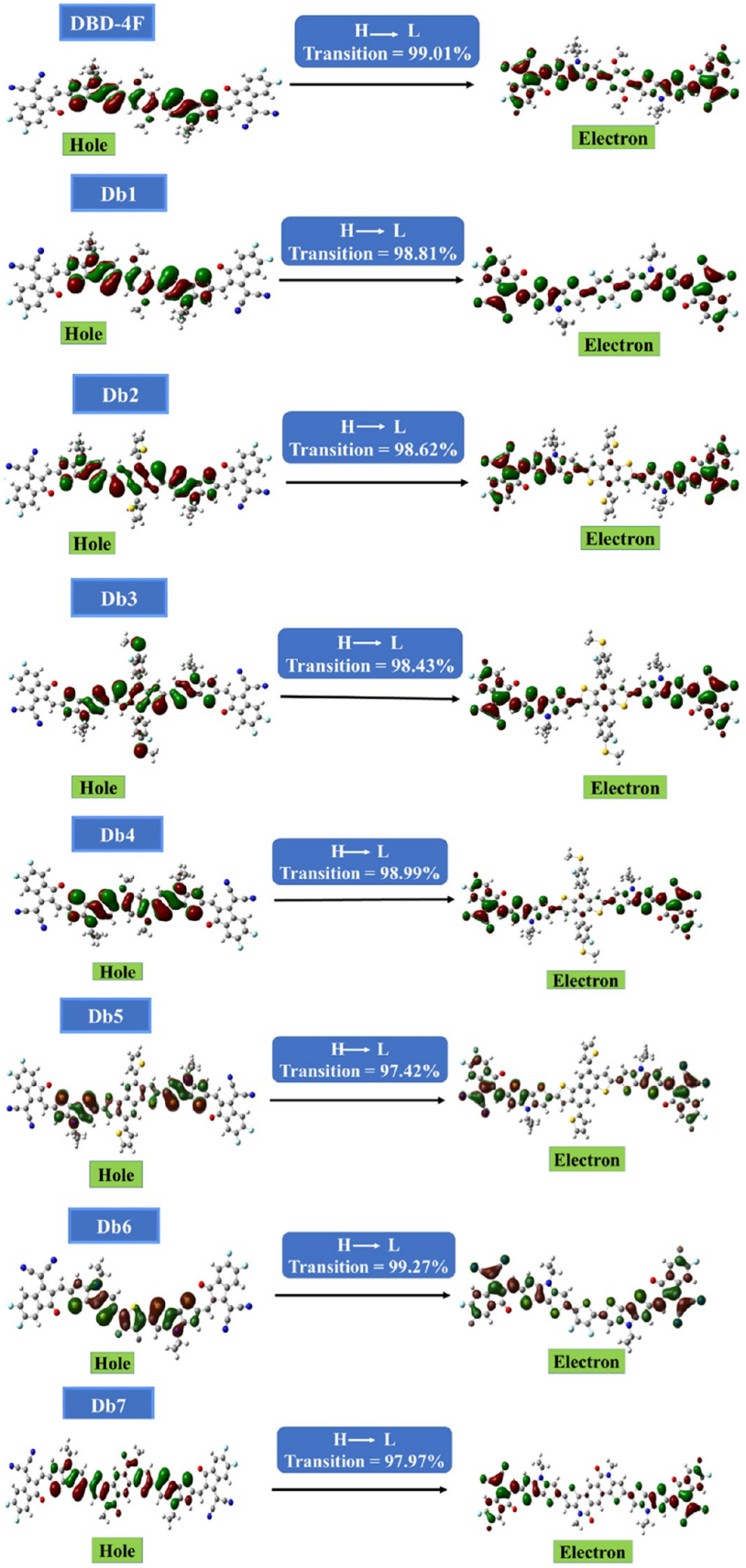

Figure 6. Representation of percentages of electron transitions from HOMO to LUMO by natural transition orbitals.

chromophores have comparable EA and IP values. All newly designed molecules possess higher EA values compared to the DBD-4F molecule. The higher values for EA reflect that these compounds have improved the ability to inject electrons into

https://doi.org/10.1021/acsomega.3c09215
ACS Omega 2024, 9, 29205−29225

Table 3. Calculated Values of Ionization Potential and Electron Affinity of the Reference and All Designed Molecules

Molecules	IP (eV)	EA (eV)
DBD-4F	6.10	2.54
Db1	6.25	2.66
Db2	5.98	2.61
Db3	6.25	2.74
Db4	5.98	2.58
Db5	5.98	2.58
Db6	6.25	2.72
Db7	5.98	2.69

their LUMO. Db3 has the maximum EA (2.74 eV), resulting in better electron transport. Compared to a reference molecule, the low IP values for Db2, Db4, Db5, and Db7 indicate a lower barrier for hole transport in these molecules. Thus, results indicate the better and improved properties of designed molecules for charge transfer, which can lead to the development of improved photovoltaic devices.

3.5. Density of States. DOS analysis is compulsory to understand the contribution of molecular fragments to form FMOs. The percentage analysis of different subunits in a molecule in increasing the HOMO and LUMO values is usually determined by DOS analysis. By employing the B3LYP/6-31G(d,p) level of theory, the arrangement of frontier molecular orbitals (FMOs) is analyzed in terms of Mulliken charge density.[52−55] Thus, calculations of DOS of all modified and reference molecules are obtained, and ultimately, plots are created by utilizing PyMolyze 1.1 software. In the DOS plot, the energy of orbitals in eV is represented on the *x*-axis, and relative intensity is expressed on the *y*-axis.[56] In this graphical analysis, there are three fragments of a molecule, namely, an acceptor, a spacer, and a core, represented by red, green, and blue lines accordingly. The total participation of these moieties to form FMOs is indicated by black lines for DBD-4F and Db1−Db7 molecules, as shown in Figure 7, and results are mentioned in Table 4. In these particular plots, the peaks onto the right side of the planar zone or band gap (E_g) on the *x*-axis manifest LUMO energy levels, while the left side exhibits energy levels of HOMO.

Results manifest that the central core of reference (DBD-4F) has 20.6% participation in increasing the HOMO, while it has just 6.9% participation in uplifting the LUMO. In DBD-4F, spacer involvement in increasing HOMO and LUMO of the molecule is 56.5 and 34.5%, respectively. The acceptor involvement in increasing HOMO and LUMO is 22.9 and 58.6%, respectively. Thus, the spacer and core moieties are more dominant in the development of HOMO. At the same time, the acceptor is dominant in LUMO, which exhibits the charge flow from a donor to an acceptor (HOMO to LUMO) and ultimately enhances the efficiency of OSCs. Almost all molecules' donor and spacer fragments uplift the HOMO level, while acceptors boost the LUMO level. HOMO acts as donor parts. Hence, the charge flow occurs from electron-donating units at the central region toward electron-withdrawing units at terminal parts in LUMO.[57−59] The Db5 molecule shows the highest acceptor participation (59.4%) in uplifting the LUMO charge density and hence can act as a better acceptor in the BHJ layer of OSCs.

3.6. Absorption Profile. To predict the consequences of central core modification on the optoelectronic properties of newly presented molecules in solvent and gaseous states, various optical parameters were studied. Simulated results are shown in Tables 5 and 6 and graphically displayed in Figure 8. All of the compounds under analysis have an absorption in the spectral range of 350−1400 nm in both solvent and gaseous phases. The DBD-4F molecule under the gaseous phase exhibited λ_{max} at 675 nm, while it showed λ_{max} at 736 nm in chloroform. The λ_{max} range of Db1−Db7 molecules in the gaseous phase ranges from 642 to 728 nm, while in the solvent phase, it ranges from 684 to 776 nm. Findings determined that the Db7 molecule showed the maximum absorption wavelength in gaseous and solvent phases at 728 and 776 nm, respectively. Having increased conjugation, Db7 also contains O, N, and S atoms in its central core portion. In Db7, n−π^* transitions also occur alongside $\pi-\pi^*$, which play a crucial role in shifting the absorption maxima toward a higher wavelength region.

A bathochromic shift was observed in Db4, Db6, and Db7 molecules than the reference molecule with increases of 5−40 nm in the solvent phase. It confirms that smaller central units, i.e., "1,4-dimethoxybenzene" in Db4 and "3,4-difluorothiophene" in Db6, are very effective moieties for causing a red shift. Whereas, in the gaseous phase, Db2, Db4, Db6, and Db7 revealed the bathochromic shift of 1−53 nm. The maximum absorption is shown by the Db7 molecule having a λ_{max} of 776 nm in chloroform. The relationship between the band gap (E_g) and the wavelength is inverse. The band gap is inversely proportional to the wavelength of maximum absorption, so a decrease in the band gap will increase λ_{max}, and thus, molecules resultantly show a bathochromic shift (red shift).[60,61] Furthermore, as indicated by Figure 8, the newly designed molecules show absorption in a broader range as compared to reference molecules, which makes them a superior choice to be used for the development of improved photovoltaic devices in the future.

3.7. Excitation Energy. The least quantity of energy required to move an electron from the ground to an excited state of a molecule is typically referred to as the excitation energy. It is related to the band gap of molecules, as the higher band gap of a molecule corresponds to the higher energy required to excite the electrons. The molecules that exhibit the lower E_x tend to show better and easier charge transfer, i.e., E_x and charge transfer have the inverse relation.[62,63] Determining the excitation energy can give fruitful information for determining the photoelectronic characteristics. Using TD-SCF simulations, E_x is determined for the entitled compounds in the solvent and gas states, and results are summarized in Tables 5 and 6, respectively. Compared to DBD-4F and other presented molecules, the Db7 molecule has the smallest E_x, demonstrating its highest electronic transition and largest charge-transfer capability.

The increasing order of E_x values for all molecules under investigation in the gas phase is Db5 > Db1 > Db3 > Db2 > DBD-4F > Db4 > Db6 > Db7. The designed molecules follow the same trend in the chloroform solvent. Db4, Db6, and Db7 have lower E_x values than those of DBD-4F, indicating greater mobility of charges in these molecules. As E_x highly depends on the band gap, it is more facile for charges to go under excitation in moieties with lower energy gaps by absorbing a minimal amount of energy. There is the highest probability of n−π^* transitions in the Db7 molecule, and these transitions require the least amount of energy, so the Db7 molecule has the lowest value of E_x due to the presence of the O, N, and S atoms. Db7 exhibits the lowest excitation energy with values of 1.59 eV in the solvent and 1.70 eV in the gaseous phase. It is also attributed to the smallest band gap of the Db7 molecule, demonstrating its highest electronic transitions and largest charge-transfer

https://doi.org/10.1021/acsomega.3c09215
ACS Omega 2024, 9, 29205−29225

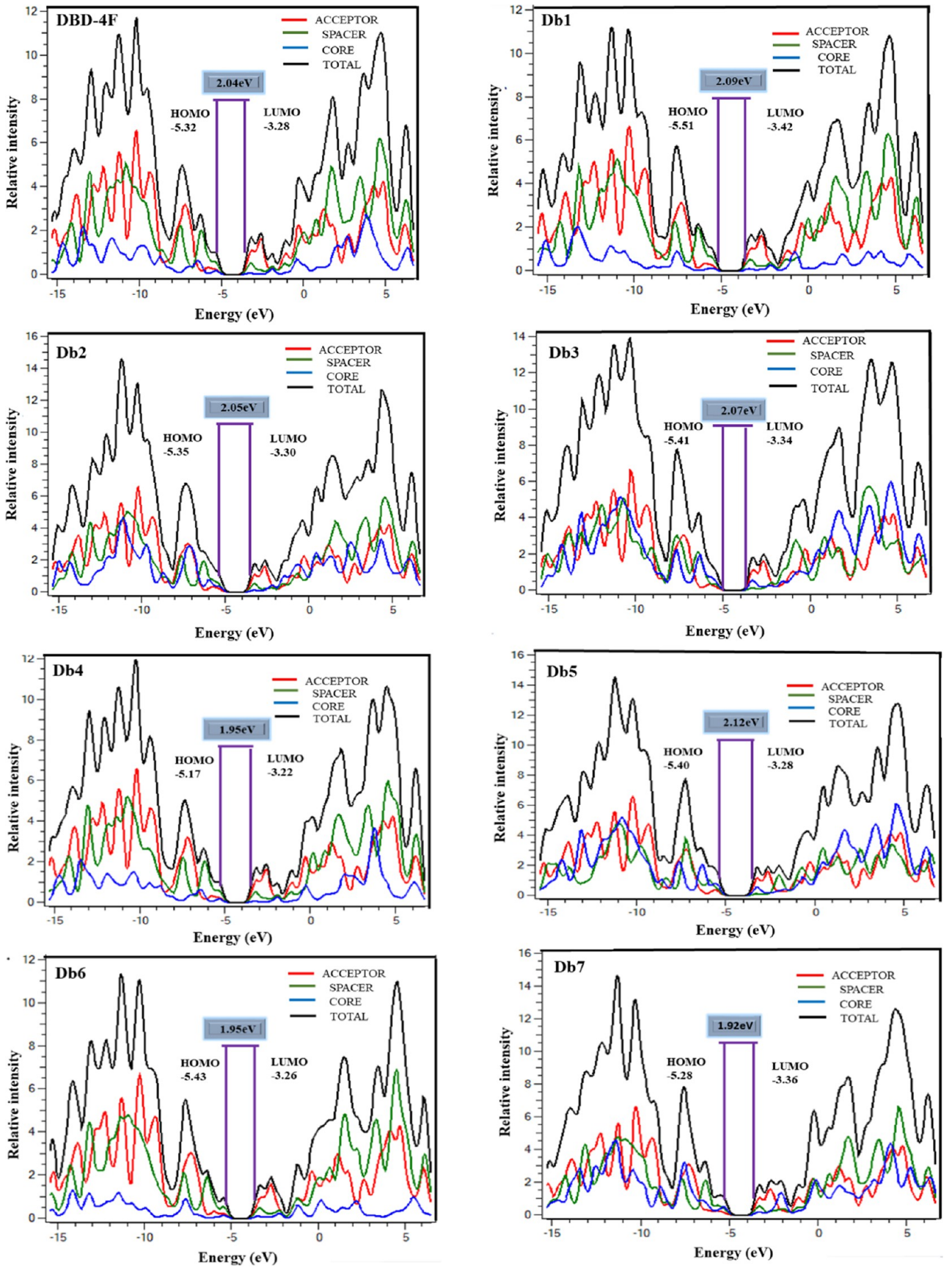

Figure 7. Plots of the density of states for DBD-4F and designed molecules Db1−Db7.

https://doi.org/10.1021/acsomega.3c09215
ACS Omega 2024, 9, 29205−29225

Table 4. Extent of the Acceptor, Spacer, and Core Percentage Contributions in HOMO and LUMO

molecules	excitation energy state	contribution of acceptor (%)	contribution of spacer (%)	contribution of core (%)
DBD-4F	HOMO	22.9	56.5	20.6
	LUMO	58.6	34.5	6.9
Db1	HOMO	25.2	61.9	9.6
	LUMO	55.2	35.5	12.8
Db2	HOMO	17.6	43.7	38.8
	LUMO	56.6	32.8	10.7
Db3	HOMO	18.6	35.3	46.1
	LUMO	56.4	10.7	32.9
Db4	HOMO	23.2	56.7	20.1
	LUMO	57.9	34.8	7.3
Db5	HOMO	19.6	32.9	47.5
	LUMO	59.4	8.60	32.0
Db6	HOMO	23.5	58.9	17.6
	LUMO	52.5	36.7	10.8
Db7	HOMO	13.4	34.4	52.2
	LUMO	53.2	32.2	14.6

Table 5. Maximum Absorption, Excitation Energy, Oscillator Strength, and Dipole Moment of the Reference and All Designed Moieties in the Chloroform Solvent

molecules	exp. λ_{max} (nm)	calculated λ_{max} (nm)	excitation energies E_x (eV)	oscillator strength (f)
DBD-4F	731	736	1.6854	3.0679
Db1		706	1.7567	3.4557
Db2		725	1.7096	3.2004
Db3		715	1.7346	3.3160
Db4		741	1.6734	3.1537
Db5		684	1.8115	3.2600
Db6		759	1.6326	3.3412
Db7		776	1.5972	3.5138

Table 6. Values of Maximum Absorption, Excitation Energy, Oscillator Strength, Dipole Moment of the Reference and All Designed Moieties in the Gaseous Medium

molecules	calculated λ_{max} (nm)	excitation energies E_x (eV)	oscillator strength (f)	%ETC
DBD-4F	676	1.835	2.8690	99.01
Db1	656	1.888	3.2240	98.81
Db2	677	1.836	2.9230	98.62
Db3	667	1.860	3.0456	98.43
Db4	679	1.826	2.9583	98.99
Db5	642	1.929	2.9185	97.42
Db6	699	1.773	3.1140	99.27
Db7	728	1.702	3.2399	97.97

capability. In light of these outcomes, it can be concluded that central core substitution on the chosen structure was a successful strategy to boost optical properties.

3.8. Oscillator Strength. A stronger oscillator strength signifies increased electronic transitions and a greater possibility that the molecule absorbs light at that specific energy level. A shift with high oscillator strength leads to a more efficient electronic transition from the ground state (HOMO) to the excited state (LUMO) in both solvent and gas phases.[64,65] The tabulated values for oscillator strength in $CHCl_3$ and gas are enlisted in Tables 5 and 6, respectively. All designed molecules have improved electronic transitions, as they have higher oscillation strength than reference. Db7 possesses the highest

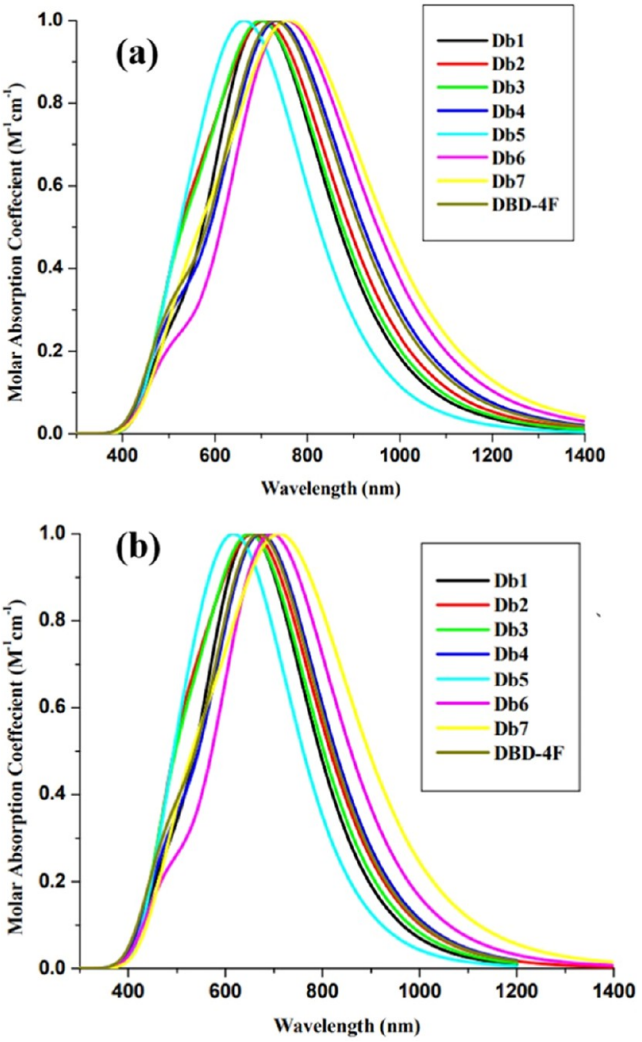

Figure 8. Graphical representation of absorption in DBD-4F and (Db1−Db7) molecules in the solvent (chloroform) phase (a) and molecules in the gaseous phase (b).

oscillator strength in both studied phases, thus showing optoelectronic properties better than those of other molecules. Db7 has an extended conjugation length as well as electron-donating $-CH_3$ groups, and both of these factors participate in improving the oscillator strength of the molecule. Furthermore, a reduced energy gap in other molecules is also vital for improving their oscillator strength. Tables 5 and 6 show that all molecules have higher oscillator strengths in the solvent than in the gas phase, indicating that these molecules are solution-processable.

3.9. Light-Harvesting Efficiency. Light-harvesting efficiency (LHE) is a measure of how well an OSC molecule can absorb and convert sunlight into electricity. LHE is significantly related to oscillator strength, ultimately affecting the production of short-circuit current (J_{sc}). Thus, the efficiency of solar devices is highly influenced by their ability to harvest sunlight.[66,67] Equation 5 was used to calculate the LHE of all currently studied molecules.[68]

$$\mathrm{LHE} = 1 - 10^{-f} \tag{5}$$

where "f" corresponds to the oscillator strength in the solvent phase of molecules. The calculated values for the LHE of studied molecules are listed in Table 7. The increasing order of these

https://doi.org/10.1021/acsomega.3c09215
ACS Omega 2024, 9, 29205−29225

Table 7. Computationally Calculated Light-Harvesting Efficiency of All of the Molecules under Consideration

molecules	oscillator strength (f)	LHE (eV)
DBD-4F	3.0679	0.9991
Db1	3.4557	0.9996
Db2	3.2004	0.9993
Db3	3.3160	0.9995
Db4	3.1537	0.9992
Db5	3.2600	0.9994
Db6	3.3412	0.9995
Db7	3.5138	0.9996

values is DBD-4F < Db4 < Db2 < Db5 < Db6 = Db3 < Db1 = Db7. All studied molecules have higher light-harvesting efficiency as compared to DBD-4F. In determined data, modified molecules Db1 (0.9996 eV) and Db7 (0.9996 eV) exhibit the highest LHE due to the high oscillator strength than other molecules. The improved LHE values of all newly presented molecules satisfy one of the requirements for constructing efficient devices in the future.

3.10. Dipole Moment. Crystallinity and solubility are the most crucial factors affected by the dipole moment to observe the polarization phenomenon in organic photovoltaic cells. Large dipole moments lead to tight molecular packing, and consistent charge transfer is possible by planar and organized structures. A larger dipole moment also increases the molecular solubility in organic solvents and plays a major role in proficient solar cell manufacturing. Thus, it enhances crystallinity as well as solubility.[59,69]

Table 8 shows the computationally tabulated values of the dipole moment of DBD-4F and Db1−Db7 molecules in both

Table 8. List of Dipole Moments of the Reference and Designed Molecules in the Solvent and Gaseous Phases

molecules	dipole moment (D) in the gas phase	dipole moment (D) in the solvent phase
DBD-4F	0.09060	0.036421
Db1	2.57980	0.036421
Db2	1.32419	3.242961
Db3	0.08429	1.628258
Db4	0.31983	0.042140
Db5	3.24173	0.323681
Db6	0.10082	4.182702
Db7	2.80745	0.049020

the solvent and gaseous phases. The decreasing order of dipole moments in the gas phase is Db5 > Db7 > Db1 > Db2 > Db4 > Db6 > DBD-4F > Db3. Db3 shows the lowest value of dipole moment, which means that the large central core portion and peripheral moieties balance the separation of charge throughout the surface of this molecule. On the other hand, in the solvent phase, the dipole moment of molecules under consideration follows decreasing order as Db6 > Db2 > Db3 > Db5 > Db7 > Db4 > DBD-4F = Db1, respectively. The dipole moment values are higher in the solvent than in the gas phase, indicating the better solubility of designed molecules in a solvent. In $CHCl_3$, all planned molecules have enhanced dipole moment values compared to the DBD-4F molecule. Db1 has a similar dipole moment value (0.036421 D) as possessed by the reference in the solvent medium. The Db6 molecule contains the highest dipole moment (4.182702 D), which can contribute toward improving charge mobility in this molecule. An increased dipole moment in newly designed molecules can be helpful for improving charge mobility up to a certain extent in these molecules, which is vital for enhancing photovoltaic efficiency.

3.11. Molecular Electrostatic Potential (MEP). MEP represents a three-dimensional (3D) charge dispersion within the molecule, particularly highlighting the electron-poor (acceptor) and electron-rich (donor) sites. In the distinctive MEP maps, the red color suggests that the area has a negative potential with extreme electron existence. On the other hand, the green color exhibits the neutral zone, and the blue regions indicate the sites with a lower presence of electron concentration.[70,71]

Figure 9 gives a pictorial representation of MEP plots of all studied molecules. On MEP maps, the oxygen atom emerges in dark red at the terminal acceptors, stipulating massive electron density in that particular zone. Furthermore, the nitrogen atom within the spacer attached to the peripheral acceptors also indicates the red color exhibiting the high existence of electrons. Within the designed molecules, the donor part that accommodates the nitrogen or oxygen atoms also proclaims the occupancy of electrons with an illuminating red color indication. The thiophene rings, the pyrrole fused ring within two thiophene rings, and methyl groups intimate blue color due to the scarcity of electrons on these targeted sites. The distinct separation between cyan and red color over a substantial portion of all planned molecules suggests improved charge separation, which makes the molecules we designed more effective materials to improve the optoelectronic characteristics in BHJ OSCs.

3.12. Transition Density Matrix (TDM) and Exciton Binding Energy. TDM is a mandatory analysis to predict the qualitative data about two-dimensional exciton's (electron−hole) movements among donor and acceptor locality within the conjugated geometry of molecules. Through this analysis, charge transitions, charge locations, and electron mobility during the excitation phenomenon can be analyzed. To have an entire comprehension of the mobility of the charge within the molecule and the extent of delocalization and resonance, a TDM plot is generally utilized. Participation of hydrogen atoms is ignored owing to their trivial impact on charge-transfer abilities. The bottom x-axis and the left y-axis represent the sequence of atoms (except H atoms) in the molecule.[72,73] The multicolored bar on the right y-axis demonstrates the charge density coefficient. The molecules have been divided into three parts to perform calculations for the transition pathway; these parts are the acceptor (A), spacer (S), and core (C).

From Figure 10, it is clear that in all of the scrutinized molecules (Db1−Db7) and reference molecules, the electron density is disseminated onto the whole molecule. The strong dispersion along the diagonals in these plots shows the $\pi-\pi^*$ electronic transitions and reveals the hole and electron coherence in donor and acceptor units. The diagonal bright spots indicate the abundant transition sites. By subsequent conjugation, charge dispersal from the donor moiety to acceptor regions is seen, leading to the smooth and efficient transfer of electrons.[74]

The interaction coefficient gives information about the possible coupling of electrons and holes. An inverse relationship lies between the interaction coefficient and charge carriers' coupling. The decreasing sequence of interaction coefficient values of the suggested molecules is Db5 > Db1 > Db3 > Db2 > DBD-4F > Db4 > Db6 > Db7, and the values are mentioned in Table 9. Db7 has the lowest interaction coefficient value (0.6942), exhibiting a smooth and efficient charge-transferring

https://doi.org/10.1021/acsomega.3c09215
ACS Omega 2024, 9, 29205−29225

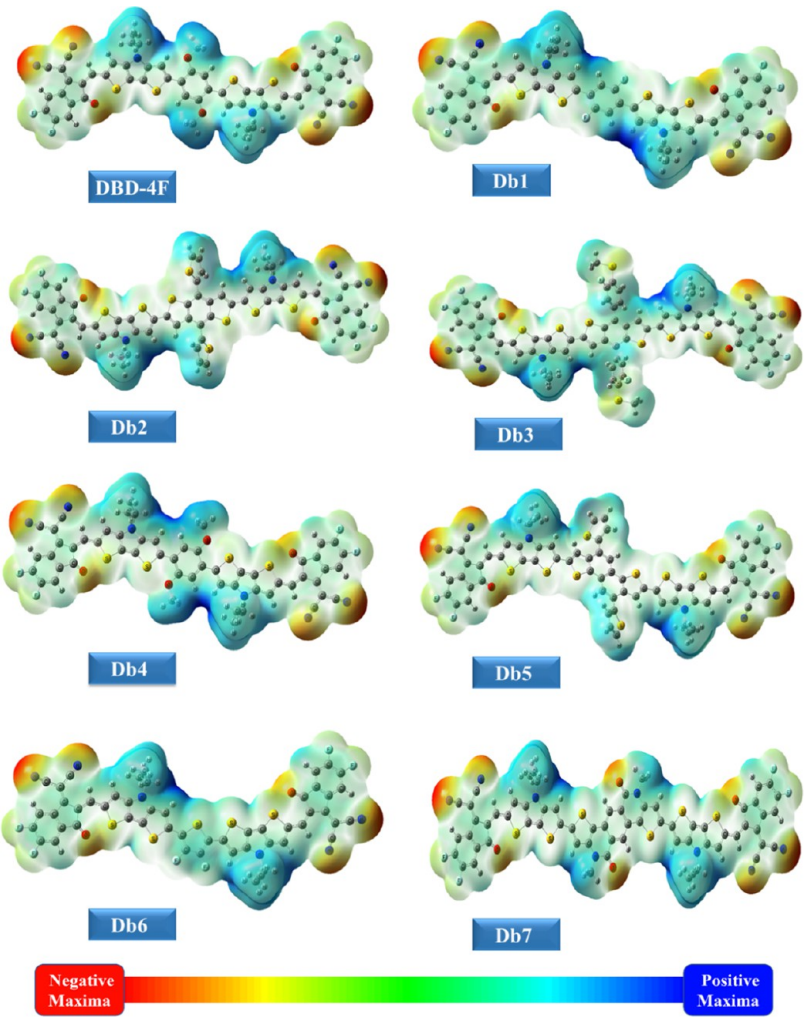

Figure 9. MEP-shaded maps of the reference and newly manufactured molecules.

phenomenon from donor to acceptor regions within the molecule. Db5, Db3, and Db2 have moieties outside the central plane, which can affect the overall movement of charges across the molecules. Db7 has the lowest energy gap and a very planar structure, so it is quite easy for charges to move toward an excited state. This behavior of Db7 indicates the greater mobility of charges and less recombination.

Exciton binding energy (E_b) is also a potent factor to consider. It is a phenomenon to generate the coulombic force within the charge carriers of conjugated molecules during photoexcitation. Where there are fewer coulombic interactions among molecular electron−hole pairs, it means that they have lesser binding energies. It results in easier movement of charges toward their respective electrodes. Equation 6 is employed for the calculations of the exciton binding energy of all molecules.[75]

$$E_b = E_g - E_x \tag{6}$$

In eq 6, E_x is the first excitation energy. The examined values for E_b of the reference and designed molecules are listed in Table 9. The increasing order of binding energies is Db6 < Db4 < DBD-4F < Db1 < Db7 < Db2 < Db3 < Db5 in the gas phase. It can be observed that the binding energy values of all molecules are comparable to each other in the gas phase. Db6 has the lowest value of E_b in the gas phase (0.176 eV), which ultimately leads to the possible diffusion of the exciton into independent charge moieties. While in the solvent phase, the increasing order of E_b of all of these molecules is Db7 < Db6 < Db5 < Db2 < Db1 < Db3 < DBD-4F < Db4. Db7 possesses the lowest value of binding energy (0.312 eV) in the chloroform solvent due to the lowest band gap and excitation energy, which manifests improved charge ability in Db7 molecules. The values of E_b of all molecules are higher in CH_3Cl than in the gaseous phase because of the solvent's strong interactions with excitons. Overall, Db6 possesses a lower binding energy than the reference in both states, indicating its better performance than the reference.

3.13. Noncovalent Interactions Analysis. NCI (noncovalent interactions) analysis evaluates and visualizes all interactions based on a reduced density gradient (RDG). The two-dimensional (2-D) reduced density graph is particularly related to the noncovalent interactions among molecules, distinguishing hydrogen bonds, weak van der Waals forces of attraction, and steric repulsive interactions. To generate the corresponding colored RDG scatter plots and 3D isosurfaces of the title molecules, Multiwfn 3.8 software was utilized. NCI revealed two related interactions: favorable and unfavorable, which can be distinguished by the product of the second eigenvalue of the Hessian matrix with density, i.e., $(\lambda_2)\rho$.

The RDG scatter graph exhibited three regions concerning sign values $(\lambda_2)\rho$.[76−79] The evaluated values of $(\lambda_2)\rho$ developed from the RDG graphs exhibit characteristics in the following way, i.e., for repulsive interactions, the $(\lambda_2)\rho$ must be greater

https://doi.org/10.1021/acsomega.3c09215
ACS Omega 2024, 9, 29205−29225

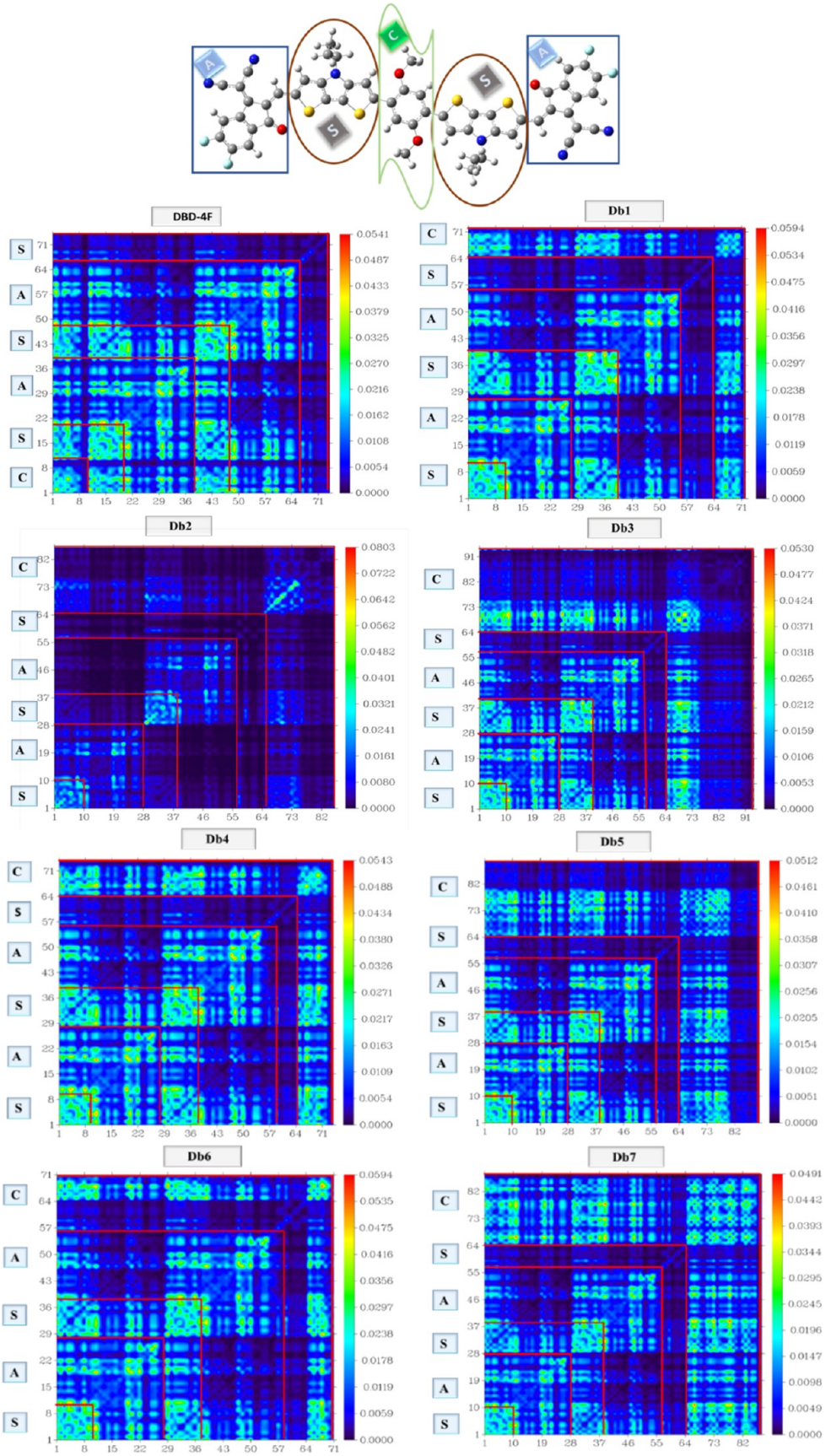

Figure 10. TDM plots of DBD-4F and all constructed molecules of Db1−Db7.

https://doi.org/10.1021/acsomega.3c09215
ACS Omega 2024, 9, 29205−29225

Table 9. Band-Gap Binding Energy in the Gaseous Phase and the Chloroform Solvent along with Interaction Coefficients in the Reference and All Constructed Molecules

molecules	E_b (eV) gaseous	E_b (eV) solvent	interaction coefficient
DBD-4F	0.195	0.344	0.7001
Db1	0.201	0.333	0.6986
Db2	0.208	0.330	0.6970
Db3	0.209	0.335	0.6961
Db4	0.194	0.346	0.6827
Db5	0.210	0.328	0.6894
Db6	0.176	0.317	0.7010
Db7	0.207	0.312	0.6942

than zero $(\lambda_2)\rho > 0$, which is represented by red color, while for the attractive interactions (hydrogen bonding), it must be lesser than zero $(\lambda_2)\rho < 0$, which is characterized by a blue region. The third zone in green color represents the weak van der Waals forces of attraction with the sign $(\lambda_2)\rho$ closest to zero. The NCI analysis was performed with a range of RDG isosurface from −0.035 to 0.02 au, as shown in Figure 11.[80−82]

In 2D NCI graphs in Figure 11, it can be seen that left- and right-sided spikes exhibited more negative and positive signs containing values of −0.05 and +0.05 au, respectively. In these scatter plots, spikes in green, blue, and red colors indicate the presence of all types of interactions within the molecule. In these plots, the blue region is at a higher level than the red region, which indicates the presence of dominant attractive forces in these molecules and their relative stability. A large number of blue peaks can be seen in Db7, which shows stronger hydrogen bonding in this molecule, which leads to enhanced stability.

In 3D isosurface densities of RDG, repulsive interactions are present between the aromatic benzene and thiazole rings indicated by the red-colored discs. Furthermore, the weak forces of interactions (van der Waals forces) between the oxygen and hydrogen atoms (O···H) were observed by the presence of green discs. As indicated in Figure 11, the dominance of attractive forces is evident. These attractive forces confirm the stability of these molecules, which is very necessary for the development of efficient solar devices.

3.14. Reorganization Energy. Reorganization energy (RE) of molecules is usually calculated to estimate the transfer of charges, i.e., electrons' movement from a donor to an acceptor. The reorganization energy is among the most crucial factors for assessing the effectiveness of OSCs. RE has an inverse relationship to charge mobility. If the calculated value of RE of a molecule is low, there will be a high hole and electron transport.[83] RE is influenced by many factors, primarily, the geometry of cationic and anionic states. Reorganization energy exists in two types: external reorganization energy, which is linked with external environmental control, and internal reorganization energy, which is concerned with internal parameters. The study of internal reorganization energy is prioritized over external energy as it provides information regarding the reorganization energies of electrons and holes.[84]

The RE values of the holes and electrons have been determined by eqs 1 and 2, and the results are listed in Table 10. All of the newly fabricated molecules have lower values of λ_e than the values of λ_h except the DBD-4F molecule. It confidently explicates the better movement of electrons than hole transport and indicates that all fabricated molecules are acceptors in nature. The Db7 possesses the lowest λ_e (0.0039334 eV), which indicates the possibility of high charge mobility in this molecule, as a low λ_e value indicates the highest electron transfer from the absorber layer to the respective electrodes. Overall, the low values of RE of electrons in almost all of the newly designed molecules can lead to the development of efficient OSCs based on these molecules.

3.15. Photovoltaic Properties. To obtain high photovoltaic performance, open-circuit voltage performs an exorbitant role as it represents the amount of maximum voltage by an optical device when no net current is flowing through the circuit. Various factors such as the temperature of the system, incident light, and charge-transferring process have a considerate impact on V_{oc}. Open-circuit voltage can be calculated by associating the LUMO of the acceptor with the HOMO of the donor material. The energy gap between HOMO and LUMO of donor and acceptor material should be high in order to achieve a higher V_{oc} that would ultimately enhance the fill factor, which is the fundamental basis for a high PCE of solar cells.[85−88] In this particular research, the HOMO of a polymer donor (PTB7-Th) is coupled with the LUMO of proposed nonfullerene acceptors (DBD-4F, Db1−Db7) to theoretically calculate the V_{oc} of molecules. The energy onset of HOMO of the PTB7-Th donor is at −5.20 eV.[89] Equation 7 is used to calculate the V_{oc} values of designed molecules.[90]

$$V_{oc} = \frac{E_{\text{HOMO of donor}} - E_{\text{LUMO of acceptor}}}{e} - 0.3 \tag{7}$$

where "e" demonstrates the molecular charge of 1 and 0.3 that is the constant generally used to represent intersurface charge.[91,92] The calculated V_{oc} values are depicted in Table 11. Db5 has a maximum V_{oc} value of 1.67 eV in these investigated molecules. Therefore, it may ultimately boost the PCE of the OSCs. The order of calculated V_{oc} of all of the molecules is Db5 > Db4 > DBD-4F > Db2 > Db3 > Db7 > Db1 > Db6, as shown in Figure 12. Db5 exhibited the highest V_{oc} due to its high-lying LUMO energy level as compared to other molecules. Similarly, the LUMO of Db4 is also at a higher energy level than the LUMO of DBD-4F. Due to this alignment of energy levels, these molecules show improvement in V_{oc}. This shows the significance of Db5 and Db4 molecules for achieving photovoltaic devices with high efficiency.

The fill factor (FF) is also one of the most crucial factors that plays a considerable role in determining the PCE of photovoltaic systems; both parameters have a relationship in a direct manner with each other. It is computed by using eq 8.[93]

$$\text{FF} = \frac{\frac{eV_{oc}}{K_BT} - \ln\left(\frac{eV_{oc}}{K_BT} + 0.72\right)}{\frac{eV_{oc}}{K_BT} + 1} \tag{8}$$

Here, $\frac{eV_{oc}}{K_BT}$ is the normalized V_{oc}, where "e" is the standard charge always 1, K_B demonstrates the Boltzmann constant that has a value of $8.61733034 \times 10^{-5}$ eV K^{-1}, and T denotes the constant temperature of 300 K.[94,95] The calculated values of normalized V_{oc} and FF are shown in Table 11. The normalized V_{oc} and FF of the DBD-4F molecule are 62.608 and 0.9191, respectively. The molecules Db4 and Db5 exhibit higher FF values than the DBD-4F molecule, as they possess high normalized V_{OC} values of 63.381 and 64.541. The decreasing order of FF values of all constituted molecules (Db1−Db7) and reference is Db5 > Db4 > DBD-4F > Db2 > Db3 > Db7 > Db1 > Db6. Thus, these molecules have more potential for converting the captured energy into electricity and, thus, constructing efficient solar cells.

https://doi.org/10.1021/acsomega.3c09215
ACS Omega 2024, 9, 29205−29225

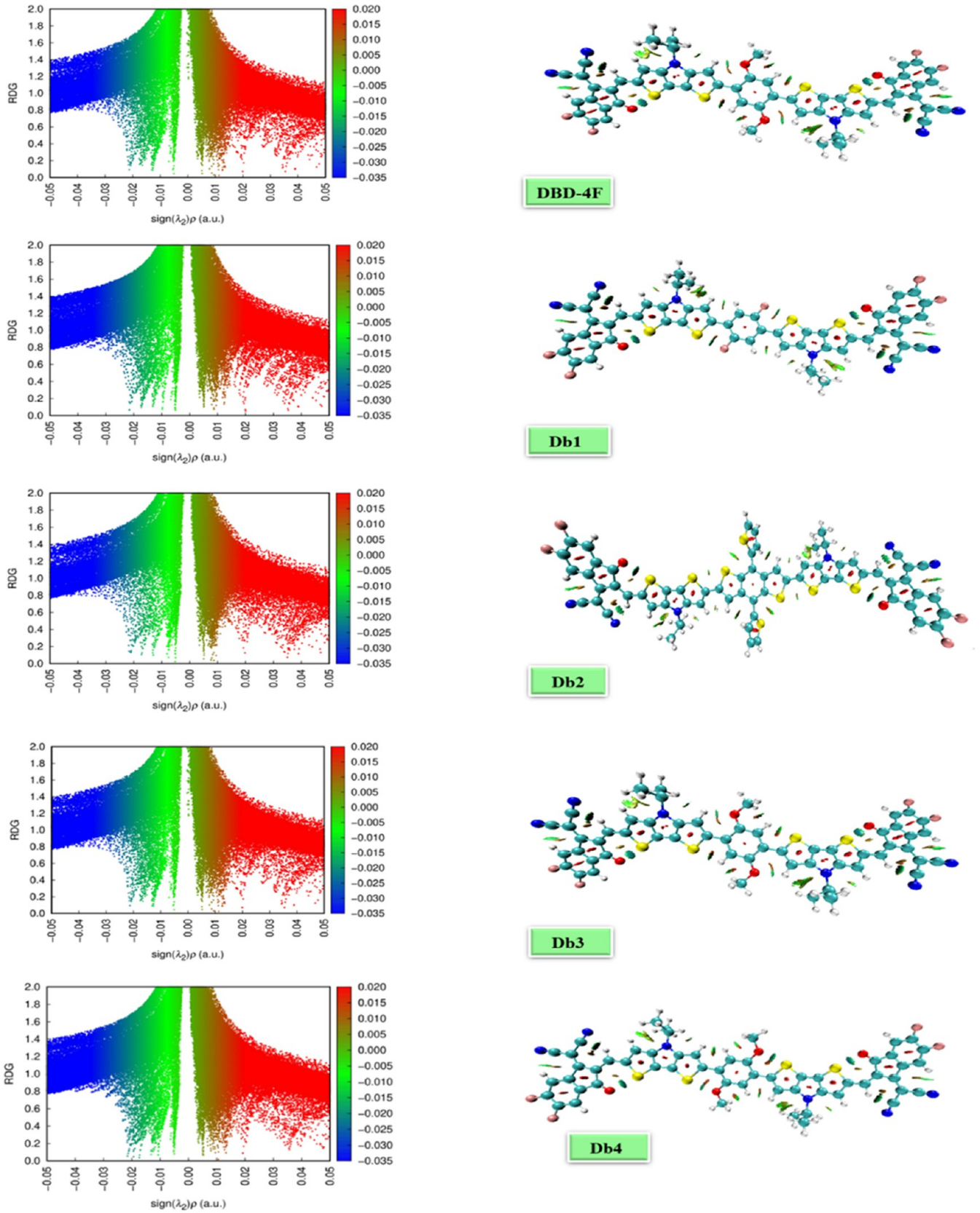

Figure 11. continued

https://doi.org/10.1021/acsomega.3c09215
ACS Omega 2024, 9, 29205−29225

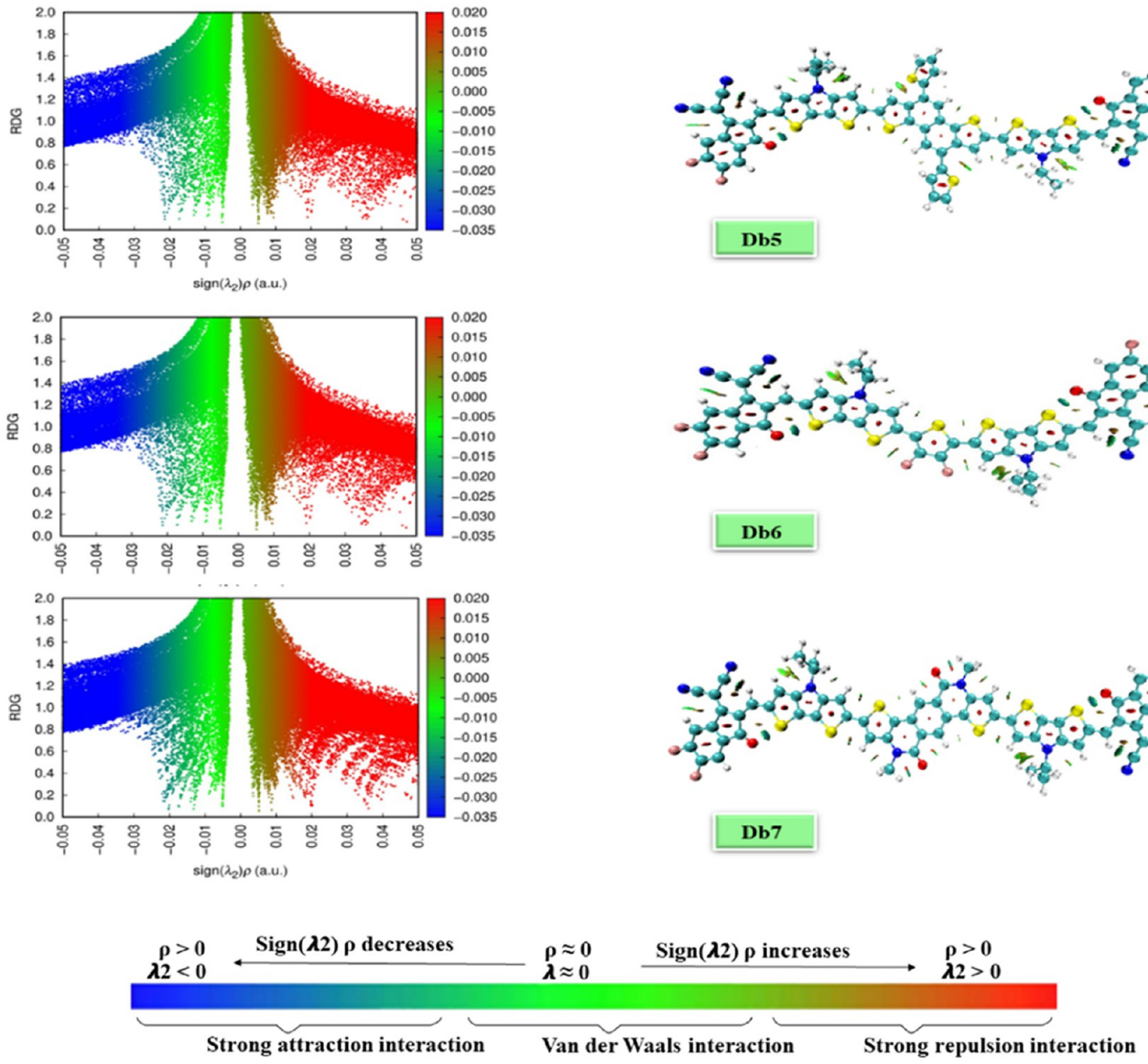

Figure 11. Representation of the strength of attractions within the molecules.

Table 10. Computationally Calculated Values of Hole and Electron Reorganization Energies for the Designed and Reference Molecules

molecules	$\lambda_{e(electron)}$ (eV)	$\lambda_{h(hole)}$ (eV)
DBD-4F	0.0056868	0.00395880
Db1	0.0054356	0.00651230
Db2	0.0053884	0.00856180
Db3	0.0056303	0.00884128
Db4	0.0056811	0.00825780
Db5	0.0040579	0.00780370
Db6	0.0064755	0.00764790
Db7	0.0039334	0.00597210

Table 11. Open-Circuit Voltage, Normalized V_{oc}, and Fill Factor of the Reference and All Constructed Molecules

molecules	V_{oc} (eV)	normalized V_{oc}	FF
DBD-4F	1.62	62.608	0.9191
Db1	1.50	57.971	0.9140
Db2	1.61	62.222	0.9187
Db3	1.59	61.449	0.9179
Db4	1.64	63.381	0.9198
Db5	1.67	64.541	0.9210
Db6	1.45	56.038	0.9117
Db7	1.53	59.130	0.9153

3.16. Charge Transfer (CT) between Donor PTB7-Th and Acceptor Db4. Studying a complex between the donor and the appropriate acceptor is an important parameter to evaluate the charge transfer. The optimal charge transfer between acceptor and donor molecules can obtain a higher photon-conversion efficiency. For assessment of charge-transfer analysis, the elected donor PTB7-Th was blended with an unfused nonfullerene-based acceptor. The Db4 designed molecule was chosen for acceptor−donor complex formation because of its bathochromic shift in absorbance, suitably low binding energy, higher V_{oc}, and lower band gap.

The depiction of charge transfer in the donor complex was exhibited parallel during optimization. This parallel orientation is suitable for an effortless charge transfer. Charge transfer between the unfused nonfullerene acceptor and donor

https://doi.org/10.1021/acsomega.3c09215
ACS Omega 2024, 9, 29205−29225

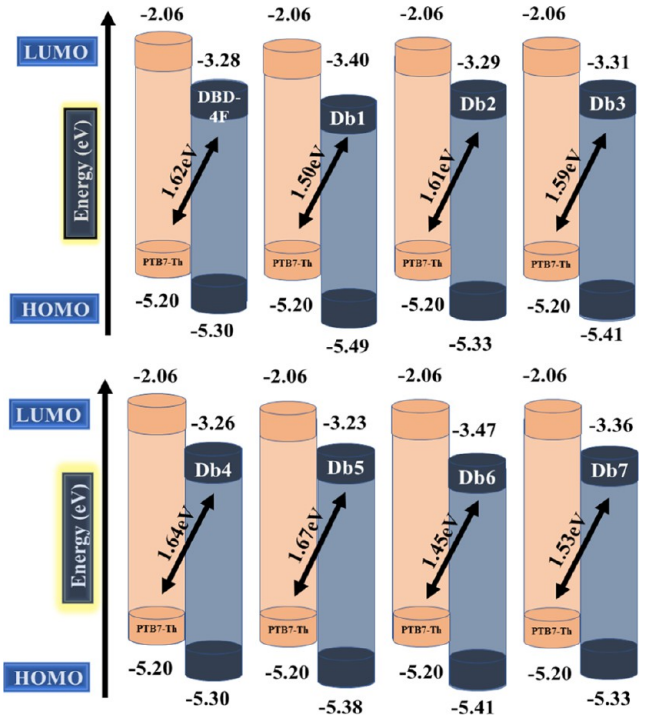

Figure 12. Difference of the energy level for DBD-4F and design molecules (Db1−Db7) concerning the donor material PTB7-TH.

molecules is illustrated in Figure 13. The FMO diagram manifested that the electronic charge density of LUMO is exhibited on the acceptor moiety (Db4). In contrast, the charge density of HOMO is located at the central core of a tiny donor molecule (PTB7-Th).[96] This indicates efficient charge transfer from a polymer donor to an acceptor molecule, thus indicating that our studied molecules are good nominees for the practical transfer of charge in organic photovoltaics.

4. CONCLUSIONS

In the ongoing research, with the resolution to upheave the productivity and cost-effectiveness of photovoltaic cells, seven new small acceptor molecules are designed theoretically by alternating the central moiety in the reference molecule. The B3LYP functional with the utilization of 6-31G(d,p) basis set is employed to inspect numerous optoelectronic characteristics, i.e., light-harvesting efficiency (LHE), the density of states (DOS), excitation energy, oscillator strength, transition density matrix (TDM), HOMO−LUMO energy levels, E_{gap}, electron affinity, ionization potential, etc. The open-circuit voltage (V_{oc}) values of all entitled molecules evaluated from the complex ranged between 1.45 and 1.67 eV, while the normalized V_{oc} and FF values ranged between 56.038 and 64.541 and between 0.9117 and 0.9210, respectively. In $CHCl_3$, the absorption maxima (λ_{max}) values of Db4 (741 nm), Db6 (759 nm), and Db7 (776 nm) are shifted toward the larger wavelengths as compared to the reference. Among all new moieties, Db6 has the smallest value of E_b, i.e., 0.176 eV in the gaseous state and 0.317 eV in the solvent state. Its excitons are easily diffused into independent charge substitutes. The Db4 molecule exhibits the lowest interaction coefficient of 0.6827, which illustrates the efficient charge-transferring process from donor to acceptor constituents of the molecule, and the Db7 molecule has the lowest band gap (E_{gap}) of 1.91 eV. The evaluated findings exhibited that the Db6 and Db7 molecules can be used for manufacturing OSCs with

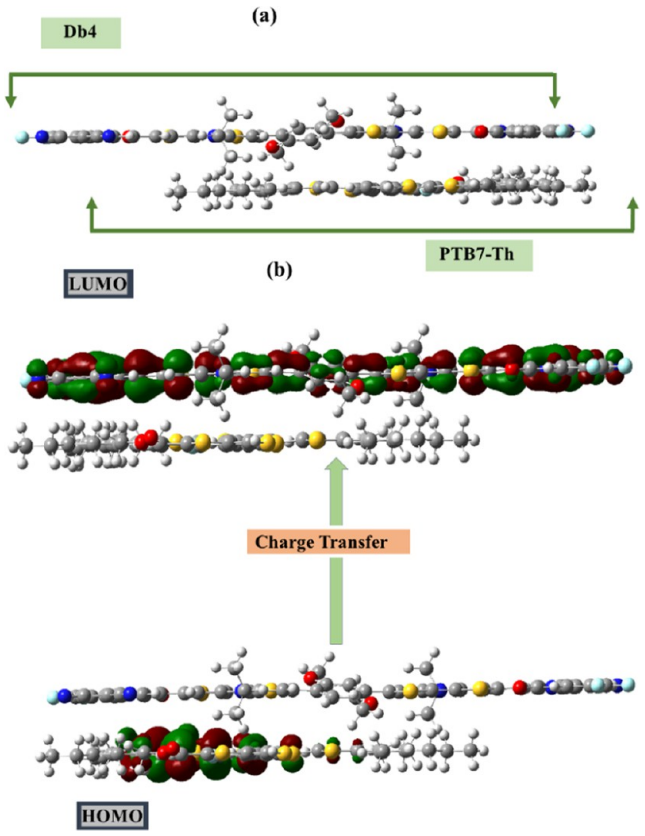

Figure 13. (a) Optimized geometry of the donor PTB7-Th and acceptor Db4 moieties. (b) Charge-transferring phenomenon from HOMO of (PTB7-Th) to LUMO of Db4.

improved optoelectronic properties as compared to pre-existing references. Furthermore, as the manufacturing of Db5 is difficult as compared to Db4, so Db4 can be a suitable option for manufacturing devices with an improved V_{oc} and fill factor.

AUTHOR INFORMATION

Corresponding Authors

Muhammad Salim Akhter − *Department of Chemistry, College of Science, University of Bahrain, Sakhir 32028, Bahrain*; Email: simsimbed@gmail.com

Ijaz Ahmad Bhatti − *Department of Chemistry, University of Agriculture, Faisalabad 38000, Pakistan*; Email: ijazchem@yahoo.com

Hadil Faris Alotaibi − *Department of Pharmaceutical Sciences, College of Pharmacy, Princess Nourah bint AbdulRahman University, Riyadh 11671, Saudi Arabia*; Email: hfalotaibi@pnu.edu.sa

Meitao Duan − *School of Pharmacy, Xiamen Medical College, Xiamen 361023, P. R. China; Research Center for Sustained and Controlled Release Agents, Xiamen Medical College, Xiamen 361023, P. R. China; Key Laboratory of Functional and Clinical Translational Medicine, Fujian Province University, Xiamen Medical College, Xiamen 361023, P. R. China*; Email: dmt@xmmc.edu.cn

Rasheed Ahmad Khera − *Department of Chemistry, University of Agriculture, Faisalabad 38000, Pakistan*; orcid.org/0000-0002-5513-8096; Email: rasheedahmadkhera@yahoo.com, rasheed.ahmad.khera@uaf.edu.pk

Ahmed Mahal − *Department of Medical Biochemical Analysis, College of Health Technology, Cihan University—Erbil, Erbil*

https://doi.org/10.1021/acsomega.3c09215
ACS Omega 2024, 9, 29205−29225

44001 Kurdistan Region, Iraq; orcid.org/0000-0002-6977-3752; Email: ahmed.mahal@cihanuniversity.edu.iq

Authors

Aamna Zulfiqar − *Department of Chemistry, University of Agriculture, Faisalabad 38000, Pakistan*

Muhammad Waqas − *Department of Chemistry, University of Agriculture, Faisalabad 38000, Pakistan;* orcid.org/0000-0002-2446-6740

Muhammad Imran − *Chemistry Department, College of Science, King Khalid University (KKU), Abha 61413, Saudi Arabia;* orcid.org/0000-0003-4072-4997

Ahmed M. Shawky − *Science and Technology Unit (STU), Umm Al-Qura University, Makkah 21955, Saudi Arabia*

Mohamed Shaban − *Department of Physics, Faculty of Science, Islamic University of Madinah, Madinah 42351, Saudi Arabia; Nanophotonics and Applications (NPA) Lab, Physics Department, Faculty of Science, Beni-Suef University, Beni-Suef 62514, Egypt;* orcid.org/0000-0002-4368-8269

Adel Ashour − *Department of Physics, Faculty of Science, Islamic University of Madinah, Madinah 42351, Saudi Arabia*

Ali S Alshomrany − *Department of Physics, College of Sciences, Umm Al-Qura University, Al Taif HWY, Mecca 24381, Saudi Arabia*

Complete contact information is available at: https://pubs.acs.org/10.1021/acsomega.3c09215

Notes

The authors declare no competing financial interest.

■ ACKNOWLEDGMENTS

This work was supported by The Science and Technology Project of Xiamen Medical College (Grant No. K2023-26) and the Key Laboratory of Functional and Clinical Translational Medicine, Fujian Province University (Grant No. XMMC-OP2023005). This work was also supported by Princess Nourah bint Abdulrahman University researchers supporting project number (PNURSP2024R205), Princess Nourah bint Abdulrahman University, Riyadh, Saudi Arabia. The authors extend their appreciation to the Deputyship for Research & Innovation, Ministry of Education in Saudi Arabia for funding this research work through the project number: IFP22U-QU4331174DSR066.

■ REFERENCES

(1) Khalid, A.; Khera, R. A.; Saeed, A.; et al. Designing benzothiadiazole based non-fullerene acceptors with high open circuit voltage and higher LUMO level to increase the efficiency of organic solar cells. *Optik* **2021**, *228*, No. 166138.

(2) Bosio, A.; Pasini, S.; Romeo, N. The history of photovoltaics with emphasis on CdTe solar cells and modules. *Coatings* **2020**, *10* (4), 344.

(3) Hachi, M.; Slimi, A.; Fitri, A.; et al. New small organic molecules based on thieno [2, 3-b] indole for efficient bulk heterojunction organic solar cells: a computational study. *Mol. Phys.* **2020**, *118* (8), No. e1662956.

(4) Hong, L.; Yao, H.; Cui, Y.; et al. 18.5% efficiency organic solar cells with a hybrid planar/bulk heterojunction. *Adv. Mater.* **2021**, *33* (43), No. 2103091.

(5) Saeed, M. U.; Iqbal, J.; Mehmood, R. F.; et al. End-capped modification of Y-Shaped dithienothiophen [3, 2-b]-pyrrolobenzothiadiazole (TPBT) based non-fullerene acceptors for high performance organic solar cells by using DFT approach. *Surf. Interfaces* **2022**, *30*, No. 101875.

(6) Waqas, M.; Iqbal, J.; Mehmood, R. F.; et al. Impact of end-capped modification of MO-IDT based non-fullerene small molecule acceptors to improve the photovoltaic properties of organic solar cells. *J. Mol. Graphics Modell.* **2022**, *116*, No. 108255.

(7) Waqas, M.; Hadia, N.; Hessien, M.; et al. End-group modification of terminal acceptors on benzothiadiazole-based BT2F-IC4F molecule to establish efficient organic solar cells. *J. Mol. Liq.* **2022**, *368*, No. 120770.

(8) Mohammad Bagher, A.; Vahid, M. M. A.; Mohsen, M. Types of solar cells and application. *Am. J. Opt. Photonics* **2015**, *3* (5), 94−113.

(9) Bai, Q.; et al. Recent progress in low-cost noncovalently fused-ring electron acceptors for organic solar cells. *Aggregate* **2022**, No. e281.

(10) Gao, H.; Han, C.; Wan, X.; et al. Recent progress in non-fused ring electron acceptors for high performance organic solar cells. *Ind. Chem. Mater.* **2023**, *1*, 60−78, DOI: 10.1039/D2IM00037G.

(11) Rani, M.; Hadia, N. M. A.; Shawky, A. M.; et al. Novel A-π-D-π-A type non-fullerene acceptors of dithienyl diketopyrropopyrrole derivatives to enhance organic photovoltaic applications: a DFT study. *RSC Adv.* **2023**, *13* (3), 1640−1658.

(12) Gao, J.; Li, Y.; Li, S.; et al. Non-fullerene acceptors with nitrogen-containing six-membered heterocycle cores for the applications in organic solar cells. *Sol. Energy Mater. Sol. Cells* **2021**, *225*, No. 111046.

(13) Cao, J.; Qu, S.; Yang, L.; et al. Asymmetric simple unfused acceptor enabling over 12% efficiency organic solar cells. *Chem. Eng. J.* **2021**, *412*, No. 128770.

(14) Liu, Z.; Feng, H.; Guo, L.; et al. A simple-structured benzo[1,2-b:4,5-b′]dithiophene-based molecule as a third component enables organic solar cells with over 18.2% efficiency. *Dyes Pigm.* **2023**, *217*, No. 111423.

(15) Fu, J.; Fong, P. W. K.; Liu, H.; et al. 19.31% binary organic solar cell and low non-radiative recombination enabled by non-monotonic intermediate state transition. *Nat. Commun.* **2023**, *14* (1), No. 1760.

(16) Gu, X.; Lai, X.; Zhang, Y.; et al. Organic Solar Cell With Efficiency Over 20% and VOC Exceeding 2.1 V Enabled by Tandem With All-Inorganic Perovskite and Thermal Annealing-Free Process. *Adv. Sci.* **2022**, *9* (28), No. 2200445.

(17) Ma, X.; Xu, W.; Liu, Z.; et al. Over 18.1% Efficiency of Layer-by-Layer Polymer Solar Cells by Enhancing Exciton Utilization near the ITO Electrode. *ACS Appl. Mater. Interfaces* **2023**, *15* (5), 7247−7254.

(18) Luo, D.; Jiang, Z.; Shan, C.; et al. Simultaneous Tuning of Alkyl Chains and End Groups in Non-fused Ring Electron Acceptors for Efficient and Stable Organic Solar Cells. *ACS Appl. Mater. Interfaces* **2022**, *14* (21), 24374−24385.

(19) Kim, M. S.; et al. High-Sensitivity Organic Photodetector Based on Surface-Concentrated Nonfused Ring Electron Acceptor. *Adv. Opt. Mater.* **2022**, No. 2202525.

(20) Zhao, F.; Dai, S.; Wu, Y.; et al. Single-junction binary-blend nonfullerene polymer solar cells with 12.1% efficiency. *Adv. Mater.* **2017**, *29* (18), No. 1700144.

(21) Huang, H.; Guo, Q.; Feng, S.; et al. Noncovalently fused-ring electron acceptors with near-infrared absorption for high-performance organic solar cells. *Nat. Commun.* **2019**, *10* (1), No. 3038.

(22) Guo, J.; Qiu, B.; Yang, D.; et al. 15.71% Efficiency All-Small-Molecule Organic Solar Cells Based on Low-Cost Synthesized Donor Molecules. *Adv. Funct. Mater.* **2022**, *32* (13), No. 2110159.

(23) Mehboob, M. Y.; Hussain, R.; Asif Iqbal, M. M.; et al. First principle theoretical designing of W-shaped Dithienosilole-based acceptor materials having efficient photovoltaic properties for high-performance organic solar cells. *J. Phys. Chem. Solids* **2021**, *157*, No. 110202.

(24) Liu, Z.; Chen, X.; Huang, S.; et al. Novel efficient accptor1-acceptor2 type copolymer donors: Vinyl induced planar geometry and high performance organic solar cells. *Chem. Eng. J.* **2021**, *419*, No. 129532.

(25) Frisch, A. *Gaussian 09W Reference*; Wallingford, USA, 2009; Vol. 470, p 25.

(26) Dennington, R.; Keith, T. A.; Millam, J. M. *GaussView 6.0. 16*; Semichem Inc.: Shawnee Mission, KS, USA, 2016.

(27) Tirado-Rives, J.; Jorgensen, W. L. Performance of B3LYP density functional methods for a large set of organic molecules. *J. Chem. Theory Comput.* **2008**, *4* (2), 297−306.
(28) Alparone, A. Response electric properties of α-helix polyglycines: A CAM-B3LYP DFT investigation. *Chem. Phys. Lett.* **2013**, *563*, 88−92.
(29) Adamo, C.; Barone, V. Exchange functionals with improved long-range behavior and adiabatic connection methods without adjustable parameters: The m PW and m PW1PW models. *J. Chem. Phys.* **1998**, *108* (2), 664−675.
(30) Fang, H.; Kim, Y. Excited-state tautomerization in the 7-azaindole-(H2O) n (n = 1 and 2) complexes in the gas phase and in solution: a theoretical study. *J. Chem. Theory Comput.* **2011**, *7* (3), 642−657.
(31) Jacquemin, D.; Preat, J.; Perpète, E. A. A TD-DFT study of the absorption spectra of fast dye salts. *Chem. Phys. Lett.* **2005**, *410* (4−6), 254−259.
(32) Klamt, A.; Moya, C.; Palomar, J. A comprehensive comparison of the IEFPCM and SS (V) PE continuum solvation methods with the COSMO approach. *J. Chem. Theory Comput.* **2015**, *11* (9), 4220−4225.
(33) Deschenes, L. A.; David, A. *Origin 6.0: Scientific Data Analysis and Graphing Software Origin Lab Corporation (formerly Microcal Software, Inc.)*; ACS Publications 2000. Commercial price: 595. Academicprice: 446. Web site: : www.originlab.com.
(34) Lu, T.; Chen, F. Multiwfn: A multifunctional wavefunction analyzer. *J. Comput. Chem.* **2012**, *33* (5), 580−592.
(35) ul Ain, Q.; Shehzad, R. A.; Yaqoob, U.; et al. Designing of benzodithiophene acridine based Donor materials with favorable photovoltaic parameters for efficient organic solar cell. *Comput. Theor. Chem.* **2021**, *1200*, No. 113238.
(36) Khan, M. I.; Hadia, N.; Shawky, A. M.; et al. Quantum mechanical modeling of fused rings-based small-donor molecules with enhanced optoelectronic attributes for high performance organic photovoltaic cells. *J. Phys. Chem. Solids* **2023**, *174*, No. 111140.
(37) Waqas, M.; Hadia, N. M. A.; Shawky, A. M.; et al. Theoretical framework for achieving high Voc in non-fused non-fullerene terthiophene-based end-capped modified derivatives for potential applications in organic photovoltaics. *RSC Adv.* **2023**, *13* (11), 7535−7553.
(38) Ishtiaq, M.; Waqas, M.; Zubair, H.; et al. Theoretical designing of symmetrical non-fullerene acceptor molecules by end-capped modification for promising photovoltaic properties of organic solar cells. *J. Mol. Liq.* **2023**, *386*, No. 122473.
(39) Majeed, M.; Waqas, M.; Mehmood, R. F.; et al. Modified optoelectronic parameters by end-group engineering of A-D-A type non-fullerene-based small symmetric acceptors constituting IBDT core for high-performance photovoltaics. *J. Phys. Chem. Solids* **2023**, *181*, No. 111495.
(40) Humphrey, W.; Dalke, A.; Schulten, K. VMD: visual molecular dynamics. *J. Mol. Graphics* **1996**, *14* (1), 33−38.
(41) Tariq, R.; Khera, R. A.; Rafique, H.; et al. Computational and theoretical study of subphthalocyanine based derivatives by varying acceptors to increase the efficiency of organic solar cells. *Comput. Theor. Chem.* **2021**, *1203*, No. 113356.
(42) Zaier, R.; Ayachi, S. DFT molecular modeling studies of D-π-A-π-D type cyclopentadithiophene-diketopyrrolopyrrole based small molecules donor materials for organic photovoltaic cells. *Optik* **2021**, *239*, No. 166787.
(43) Mubashar, U.; Farhat, A.; Khera, R. A.; et al. Designing and theoretical study of fluorinated small molecule donor materials for organic solar cells. *J. Mol. Model.* **2021**, *27* (7), 216.
(44) Pandey, S. K. Computational study on the structure, stability, and electronic feature analyses of trapped halocarbons inside a novel bispyrazole organic molecular cage. *ACS Omega* **2021**, *6* (17), 11711−11728.
(45) Ans, M.; Manzoor, F.; Ayub, K.; et al. Designing dithienothiophene (DTT)-based donor materials with efficient photovoltaic parameters for organic solar cells. *J. Mol. Model.* **2019**, *25*, 1−12.
(46) Abbas, F.; Ali, U.; Tallat, A.; et al. An optoelectronic study to design better benzodithiophene (BDT) donor unit based non-fullerene organic solar cells (OSCs): the DFT approaches. *Chem. Pap.* **2022**, *76* (8), 4977−4987.
(47) Ali, U.; Abbas, F. An extension of electron acceptor sites around Thiazolothiazole unit for evaluation of large power conversion efficiency: A theoretical insight. *Spectrochim. Acta, Part A* **2022**, *281*, No. 121610.
(48) Sadiq, S.; Waqas, M.; Zahoor, A.; et al. Synergistic modification of end groups in Quinoxaline fused core-based acceptor molecule to enhance its photovoltaic characteristics for superior organic solar cells. *J. Mol. Graphics Modell.* **2023**, *123*, No. 108518.
(49) Hassan, A. U.; Sumrra, S. H. Exploration of pull−push effect for novel photovoltaic dyes with A−π−D design: a DFT/TD-DFT investigation. *J. Fluoresc.* **2022**, *32* (6), 1999−2014.
(50) Shang, C.; Sun, C. Substituent effects on photophysical properties of ESIPT-based fluorophores bearing the 4-diethylamino-salicylaldehyde core. *J. Mol. Liq.* **2022**, *367*, No. 120477.
(51) Ahmed, S.; Dutta, R.; Kalita, D. J. Strategical designing of diketopyrrolopyrrole-thiophene based donor-acceptor type organic oligomers and study their transport properties: A DFT/TD-DFT perspective. *Chem. Phys. Lett.* **2019**, *730*, 14−25.
(52) Ans, M.; Ayub, K.; Muhammad, S.; et al. Development of fullerene free acceptors molecules for organic solar cells: a step way forward toward efficient organic solar cells. *Comput. Theor. Chem.* **2019**, *1161*, 26−38.
(53) Khalid, M.; Shafiq, I.; Zhu, M.; et al. Efficient tuning of small acceptor chromophores with A1-π-A2-π-A1 configuration for high efficacy of organic solar cells via end group manipulation. *J. Saudi Chem. Soc.* **2021**, *25* (8), No. 101305.
(54) Maqsood, M. H.; Khera, R. A.; Mehmood, R. F.; et al. End-cap modeling on the thienyl-substituted benzodithiophene trimer-based donor molecule for achieving higher photovoltaic performance. *J. Mol. Graphics Modell.* **2023**, *124*, No. 108550.
(55) Rehman, F. u.; Waqas, M.; Imran, M.; et al. Approach toward Low Energy Loss in Symmetrical Nonfullerene Acceptor Molecules Inspired by Insertion of Different π-Spacers for Developing Efficient Organic Solar Cells. *ACS Omega* **2023**, *8*, 43792−43812, DOI: 10.1021/acsomega.3c05665.
(56) Sharif, A.; Jabeen, S.; Iqbal, S.; et al. Tuning the optoelectronic properties of dibenzochrysene (DBC) based small molecules for organic solar cells. *Mater. Sci. Semicond. Process.* **2021**, *127*, No. 105689.
(57) Khan, M. U.; Hussain, R.; Mehboob, M. Y.; et al. First theoretical framework of Z-shaped acceptor materials with fused-chrysene core for high performance organic solar cells. *Spectrochim. Acta, Part A* **2021**, *245*, No. 118938.
(58) Mehboob, M. Y.; Hussain, R.; Khan, M. U.; et al. Quantum chemical design of near-infrared sensitive fused ring electron acceptors containing selenophene as π-bridge for high-performance organic solar cells. *J. Phys. Org. Chem.* **2021**, *34* (8), No. e4204.
(59) Abbas, M.; Ali, U.; Faizan, M.; et al. Spirofluorene based small molecules as an alternative to traditional non-fullerene acceptors for organic solar cells. *Opt. Quantum Electron.* **2021**, *53* (5), 246.
(60) Iqbal, M. M. A.; et al. Designing efficient AD-A1-DA type fullerene free acceptor molecules with enhanced power conversion efficiency for solar cell applications. *Spectrochim. Acta, Part A* **2023**, *285*, No. 121844.
(61) Zahoor, A.; Sadiq, S.; Khera, R. A.; et al. A DFT study for improving the photovoltaic performance of organic solar cells by designing symmetric non-fullerene acceptors by quantum chemical modification on pre-existed LC81 molecule. *J. Mol. Graphics Modell.* **2023**, *125*, No. 108613.
(62) Zubair, H.; Mahmood, R. F.; Waqas, M.; et al. Effect of tailoring π-linkers with extended conjugation on the SJ-IC molecule for achieving high VOC and improved charge mobility towards enhanced photovoltaic applications. *RSC Adv.* **2023**, *13* (37), 26050−26068.
(63) Majeed, M.; Waqas, M.; Aloui, Z.; et al. Exploring the Electronic, Optical, and Charge Transfer Properties of A-D-A-Type IDTV-ThIC-Based Molecules To Enhance Photovoltaic Performance of Organic Solar Cells. *ACS Omega* **2023**, *8* (48), 45384−45404.

https://doi.org/10.1021/acsomega.3c09215
ACS Omega 2024, 9, 29205−29225

(64) Waqas, M.; Hadia, N.; Hessien, M.; et al. Designing of symmetrical A-D-A type non-fullerene acceptors by side-chain engineering of an indacenodithienothiophene (IDTT) core based molecule: A computational approach. *Comput. Theor. Chem.* **2022**, *1217*, No. 113904.
(65) Ali, R. et al. An Approach Towards Low Energy Loss by End-capped Modification of A2-D−A1−D−A2-type Molecules for Tuning the Photovoltaic Properties of Organic Solar Cells. *J. Comput. Biophys. Chem.* 228 1013 1040. .
(66) Hussain, R.; Adnan, M.; Irshad, Z.; et al. Environmentally compatible 3-dimensional star-shaped donor materials for efficient organic solar cells. *Int. J. Energy Res.* **2022**, *46* (15), 22145−22161.
(67) Rehman, F. U.; Hameed, S.; Khera, R. A.; et al. High-Efficiency and Low-Energy-Loss Organic Solar Cells Enabled by Tuning the End Group Modification of the Terthiophene-Based Acceptor Molecules to Enhance Photovoltaic Properties. *ACS Omega* **2023**, *8* (45), 42492−42510.
(68) Mary, Y. S.; Mary, Y. S.; Resmi, K.; et al. Detailed quantum mechanical, molecular docking, QSAR prediction, photovoltaic light harvesting efficiency analysis of benzil and its halogenated analogues. *Heliyon* **2019**, *5* (11), No. e02825, DOI: 10.1016/j.heliyon.2019.e02825.
(69) Zubair, H.; Akhter, M. S.; Waqas, M.; et al. A computational insight into enhancement of photovoltaic properties of non-fullerene acceptors by end-group modulations in the structural framework of INPIC molecule. *J. Mol. Graphics Modell.* **2024**, *126*, No. 108664.
(70) Rasool, A.; Zahid, S.; Ans, M.; et al. Bithieno thiophene-based small molecules for application as donor materials for organic solar cells and hole transport materials for perovskite solar cells. *ACS Omega* **2022**, *7* (1), 844−862.
(71) Idrees, A.; ur-Rehman, A.; Waqas, M.; et al. Strategies Toward End-group Engineering of Chrysene Core-based Non-fullerene Acceptors for High Performance Organic Solar Cells: A DFT Study. *J. Comput. Biophys. Chem.* **2023**, *22* (8), 1041−1066.
(72) Khan, M. U.; Mehboob, M. Y.; Hussain, R.; et al. Designing spirobifullerene core based three-dimensional cross shape acceptor materials with promising photovoltaic properties for high-efficiency organic solar cells. *Int. J. Quantum Chem.* **2020**, *120* (22), No. e26377.
(73) Etabti, H.; Fitri, A.; Benjelloun, A. T.; et al. Designing and theoretical study of benzocarbazole-based D-π-D type small molecules donor for organic solar cells. *J. Mol. Graphics Modell.* **2023**, *121*, No. 108455.
(74) Khan, M. U.; Khalid, M.; Khera, R. A.; et al. Influence of acceptor tethering on the performance of nonlinear optical properties for pyrene-based materials with A-π-D-π-D architecture. *Arabian J. Chem.* **2022**, *15* (3), No. 103673.
(75) Moses, D.; Wang, J.; Heeger, A. J.; et al. Singlet exciton binding energy in poly(phenylene vinylene). *Proc. Natl. Acad. Sci. U.S.A.* **2001**, *98* (24), 13496−13500.
(76) Pandey, S. K. Novel and polynuclear K-and Na-based superalkali hydroxides as superbases better than Li-related species and their enhanced properties: An ab initio exploration. *ACS Omega* **2021**, *6* (46), 31077−31092.
(77) Bouhadiba, A.; Rahali, S.; Belhocine, Y.; et al. Structural and energetic investigation on the host/guest inclusion process of benzyl isothiocyanate into β-cyclodextrin using dispersion-corrected DFT calculations. *Carbohydr. Res.* **2020**, *491*, No. 107980.
(78) Samanta, P. N.; Das, K. K. Inhibition activities of catechol diether based non-nucleoside inhibitors against the HIV reverse transcriptase variants: Insights from molecular docking and ONIOM calculations. *J. Mol. Graphics Modell.* **2017**, *75*, 294−305.
(79) Smitha, M.; Mary, Y. S.; Mary, Y. S.; et al. Modeling the DFT structural and reactivity studies of a pyrimidine-6-carboxylate derivative with reference to its wavefunction-dependent, MD simulations and evaluation for potential antimicrobial activity. *J. Mol. Struct.* **2021**, *1237*, No. 130397.
(80) Salah, M.; Belghiti, M.; Aitouna, A.; et al. MEDT Study of the 1, 3-DC Reaction of Diazomethane with Psilostachyin and investigation about the interactions of some pyrazoline derivatives with Protease (Mpro) of nCoV-2. *J. Mol. Graphics Modell.* **2021**, *102*, No. 107763.
(81) Tang, L.; Zhu, W. Molecular design, property prediction, and intermolecular interactions for high-energy cage compounds based on the skeletons of RDX and HMX. *J. Chin. Chem. Soc.* **2021**, *68* (4), 557−568.
(82) Kourat, O.; et al. Synthesis, crystal structure, Hirshfeld surface analysis, spectral characterization, reduced density gradient and nonlinear optical investigation on (E)-N′-(4-nitrobenzylidene)-2-(quinolin-8-yloxy) acetohydrazide monohydrate: A combined experimental and DFT approach. *J. Mol. Struct.* **2020**, *1222*, No. 128952.
(83) Rukhsar, J.; et al. A DFT approach toward designing selenophene-based unfused small molecule acceptors by end-capped modification for improving the photovoltaic performance of organic solar cells. *J. Phys. Org. Chem.* **2023**, *37* (3), No. e4587.
(84) Adnan, M.; Irshad, Z.; Hussain, R.; et al. Influence of End-Capped Engineering on 3-Dimenional Star-Shaped Triphenylamine-Based Donor Materials for Efficient Organic Solar Cells. *Arabian J. Chem.* **2023**, *16*, No. 104709.
(85) Jaffar, K.; Elqahtani, Z. M.; Afzal, Q. Q.; et al. Quantum chemical study of end-capped acceptor and bridge on triphenyl diamine based molecules to enhance the optoelectronic properties of organic solar cells. *Polymer* **2022**, *245*, No. 124675.
(86) Rafiq, M.; Ahmad Khera, R.; Salim, M.; et al. Tuning the optoelectronic properties of scaffolds by using variable central core unit and their photovoltaic applications. *Chem. Phys. Lett.* **2021**, *782*, No. 139018.
(87) Asif, T.; Khera, R. A.; Naveed, A.; et al. Tuning the optoelectronic properties of naphthodithiophene (NDT) for designing of ADA type photovoltaic materials. *Optik* **2021**, *247*, No. 167892.
(88) Ans, M.; Paramasivam, M.; Ayub, K.; et al. Designing alkoxy-induced based high performance near infrared sensitive small molecule acceptors for organic solar cells. *J. Mol. Liq.* **2020**, *305*, No. 112829.
(89) Iqbal, M. M. A.; Mehboob, M. Y.; Arshad, M. Quinoxaline based unfused non-fullerene acceptor molecules with PTB7-Th donor polymer for high performance organic solar cell applications. *J. Mol. Graphics Modell.* **2022**, *114*, No. 108181.
(90) Ali, S.; Akhter, M. S.; Waqas, M.; et al. End-capped engineering of Quinoxaline core-based non-fullerene acceptor materials with improved power conversion efficiency. *J. Mol. Graphics Modell.* **2024**, *127*, No. 108699.
(91) Afzal, M.; Naeem, N.; Iqbal, S.; et al. Rational design of dithieno [2, 3-D: 2′, 3′-D′]-benzo [1, 2-B: 4, 5-B′] dithiophene based small molecule donor for plausible performance organic solar cell. *Opt. Quantum Electron.* **2023**, *55* (1), 1−20.
(92) Luo, D.; Jin, R. Theoretical characterisation and design of D−π−A star-shaped molecules with triphenylamine as core and diketopyrrolopyrroles as arms for organic solar cells. *Mol. Phys.* **2019**, *117* (14), 1825−1832.
(93) Ans, M.; Iqbal, J.; Eliasson, B.; et al. Designing of non-fullerene 3D star-shaped acceptors for organic solar cells. *J. Mol. Model.* **2019**, *25*, 1−12.
(94) Roy, J. K.; Kar, S.; Leszczynski, J. Insight into the optoelectronic properties of designed solar cells efficient tetrahydroquinoline dye-sensitizers on TiO2 (101) surface: first principles approach. *Sci. Rep.* **2018**, *8* (1), No. 10997.
(95) Zaier, R.; De La Cruz, M. P.; De La Puente, F. L.; et al. Optoelectronic properties of cyclopentadithiophene-based donor−acceptor copolymers as donors in bulk heterojunction organic solar cells: A theoretical study. *J. Phys. Chem. Solids* **2020**, *145*, No. 109532.
(96) Naeem, N.; Tahir, T.; Ans, M.; et al. Molecular engineering strategy of naphthalimide based small donor molecules for high-performance organic solar cells. *Comput. Theor. Chem.* **2021**, *1204*, No. 113416.

https://doi.org/10.1021/acsomega.3c09215
ACS Omega 2024, 9, 29205−29225